Natural Resources Canada
Ressources naturelles Canada

Interpretations and implications of preliminary LA ICP-MS analysis of chert for the origin of geochemical signatures in banded iron-formations from the Meadowbank gold deposit, western Churchill Province, Nunavut

B. Gourcerol, P.C. Thurston, D.J. Kontak, and O. Côté-Mantha

Geological Survey of Canada
Current Research 2014-1

2014

Canada

Geological Survey of Canada
Current Research 2014-1

Interpretations and implications of preliminary LA ICP-MS analysis of chert for the origin of geochemical signatures in banded iron-formations from the Meadowbank gold deposit, western Churchill Province, Nunavut

B. Gourcerol, P.C. Thurston, D.J. Kontak, and O. Côté-Mantha

2014

ISSN 1701-4387
Catalogue No. M44-2014/1E-PDF
ISBN 978-1-100-22877-8
doi:10.4095/293129

A copy of this publication is also available for reference in depository libraries across Canada through access to the Depository Services Program's Web site at http://dsp-psd.pwgsc.gc.ca

This publication is available for free download through GEOSCAN
http://geoscan.ess.nrcan.gc.ca

Recommended citation

Gourcerol, B., Thurston, P.C., Kontak, D.J., and Côté-Mantha, O., 2013. Interpretations and implications of preliminary LA ICP-MS analysis of chert for the origin of geochemical signatures in banded iron-formations from the Meadowbank gold deposit, western Churchill Province, Nunavut; Geological Survey of Canada, Current Research 2013-20, 22 p. doi:10.4095/293129

Critical review
S. Castonguay

Authors
B. Gourcerol (gourcerol.blandine@gmail.com)
P.C. Thurston (pthurston@laurentian.ca)
D.J. Kontak (dKontak@laurentian.ca)
Mineral Exploration Research Centre
Laurentian University
Sudbury, Ontario
P3E 2C6

O. Côté-Mantha (Olivier.cote-mantha@agnico-eagle.com)
Agnico Eagle Mines Ltd. – Division Exploration
Chemin de la mine Goldex
Val d'Or, Quebec
J9P 4N9

Correction date:

Interpretations and implications of preliminary LA ICP-MS analysis of chert for the origin of geochemical signatures in banded iron-formations from the Meadowbank gold deposit, western Churchill Province, Nunavut

B. Gourcerol, P.C. Thurston, D.J. Kontak, and O. Côté-Mantha

Gourcerol, B., Thurston, P.C., Kontak, D.J., and Côté-Mantha, O., 2013. Interpretations and implications of preliminary LA ICP-MS analysis of chert for the origin of geochemical signatures in banded iron-formations from the Meadowbank gold deposit, western Churchill Province, Nunavut; Geological Survey of Canada, Current Research 2013-20, 22 p. doi:10.4095/293129

Abstract: This project is designed to establish if there is a distinctive geochemical signature for the types of banded iron-formations (BIF) that contain gold mineralization and whether a hydrothermal footprint for the mineralization can be detected. Herein are reported the preliminary geochemistry results of a LA ICP-MS study of 39 chert samples for BIFs from the Meadowbank deposit in the Rae Domain of western Churchill Province where gold mineralization is associated with several Algoma-type BIFs within the Neoarchean Woodburn Lake Group. The main deposit is located in the Central BIF, which has been in production since 2010 with 24.5 Mt proven/probable ore reserves grading 2.8 g/t (2011). Recently, mineralization has also been identified associated with BIFs in the Far West, West, East and Grizzly zones. The geochemistry of the cherts from these five BIFs, as determined from line traverses of chert using the in situ LA ICP-MS method, has identified an ambient seawater signature (characterized by enrichment in HREE relative to LREE, positive La, Gd, and Y anomalies) and a hydrothermal signature (characterized by a positive Eu anomaly), with some influence of crustal contamination.

Résumé : Ce projet vise à établir si les types de formations de fer rubanées (FFR) qui contiennent une minéralisation aurifère présentent une signature géochimique caractéristique et si une empreinte hydrothermale pour cette minéralisation peut être établie. Nous présentons dans cet article les résultats préliminaires d'une étude d'analyse géochimique par ablation laser et spectrométrie de masse à plasma couplé par induction (LA ICP-MS) sur 39 échantillons de chert des FFR du gisement de Meadowbank dans le domaine de Rae de la Province de Churchill occidentale où la minéralisation aurifère est associée à plusieurs FFR de type Algoma, lesquelles sont contenues dans le Groupe de Woodburn Lake du Néoarchéen. Le principal gisement, situé dans la FFR centrale, est en production depuis 2010 et renferme 24,5 Mt de minerai (réserves prouvées et probables) titrant 2,8 g/t de Au (2011). Récemment, des minéralisations ont également été relevées dans des FFR situées dans les zones Far West, West IF, East BIF et Grizzly. La géochimie du chert de ces cinq FFR, telle qu'elle a été déterminée par analyse LA ICP-MS in situ le long de parcours transversaux dans cette lithologie, a permis d'identifier une signature d'eau de mer ambiante (caractérisée par un enrichissement en terres rares lourdes par rapport aux terres rares légères et des anomalies positives en La, Gd et Y) et une signature hydrothermale (caractérisée par une anomalie positive en Eu), avec une certaine influence de contamination crustale.

INTRODUCTION

Among mineral deposits within Archean cratons, gold mineralization from greenstone belts is economically one of the most important, representing 13% of the world's gold resources (Goldfarb et al., 2001; Dubé and Gosselin, 2007). Within the Archean-early Paleoproterozoic gold deposits, the exploited mineralization includes banded iron-formation (BIF) where the gold is associated with localized sulphide-facies zones in regionally extensive oxide-facies iron-formation. Well known iron-formation –associated gold deposits include the Homestake deposit in the Wyoming Craton (Frei et al., 2008), the Geita deposit in the Tanzanian Craton (Kuehn, 1990), Morro Velho in the Sao Francisco Craton (Ladeira, 1991) Lupin in the Slave Craton (Kerswill, 1993), Meadowbank (Sherlock et al., 2004) and Meliadine (Carpenter et al., 2005) in the Churchill Province, and Musselwhite (Hall and Rigg, 1986) and Beardmore-Geraldton (Lafrance et al., 2004) in the Superior Province.

Iron-formation in the area is classified as banded iron-formation (BIF) that originated as fine-grained chemical muds and granular iron-formation (GIF). It has detrital textures and represents well sorted sands formed by erosion and intrabasinal redeposition of chemical muds (e.g. Clout and Simonson, 2005). The BIF is classified as Superior type, laterally extensive, thick units deposited in a shelf environment generally Proterozoic in age, and Algoma-type BIF which is laterally less extensive, and thinner than the Superior type, associated with volcanic rocks and generally of Archean age (Gross, 1965).

The iron-bearing minerals in iron-formation are considered precipitates from basin waters as siderite and iron oxy-hydroxides transformed diagenetically to hematite, magnetite, various iron silicates, and pyrite. The origin of BIF chert is controversial, with the majority view being that the chert originates alternatively as a seawater precipitate (Bolhar et al., 2005; Thurston et al., 2012), a hydrothermal precipitate (Allwood et al., 2010; Thurston et al., 2012) or by replacement (Hanor and Duchac, 1990), and a minority view involving solely dissociation of iron silicates into iron oxides and colloidal silica (Lascelles, 2007).

The majority of iron-formation units represent deposition as marine units. A review by Clout and Simonson (2005) indicates that GIF units are underlain by shallow marine deposits such as tidal quartz arenites or platformal carbonates, whereas BIF are associated with deeper water shale-rich turbidites varying from siliciclastic to volcaniclastic to carbonate (Clout and Simonson, 2005). The majority of Archean BIF units are thinly laminated with rare graded beds and depositional structures such as ball-and-pillow structures and flame structures. This lack of depositional structures is interpreted to represent deposition below wave base. The ball-and-pillow structures and flame structures indicate rapid deposition of material onto partially lithified units (e.g. Baldwin, 2009). There are some Algoma-type BIF units associated with crossbedded sands which have been interpreted to represent shallow-water deposition in deltas on the margins of older continental blocks (Fralick and Pufahl, 2006). There is limited understanding at present of the variation of BIF geochemistry at a regional scale with but a single study which describes variation in the BIF at the top of the Deloro assemblage in the Abitibi greenstone belt (Thurston et al., 2012).

It is now recognized that geochemical tools, such as REE+Y systematics, indicate that chert bands in Algoma-type BIF reflect one of three processes, namely direct precipitates from seawater, a hydrothermal origin, and replacement processes (Bolhar et al., 2005; Thurston et al., 2012). An essential question, therefore, is whether the gold-mineralizing fluids have a preference for one geochemical type of iron-formation versus another. Lode-gold and BIF-hosted gold deposits are widely conceded to be epigenetic, thus, at a regional scale the geochemical signature of BIF may perhaps provide a vector toward zones with an enhanced potential to host gold mineralization.

This PhD project, entitled "The geochemical signatures of banded-iron formation (BIF), their primary geochemistry signatures, tectonic setting(s) and implications for exploration of BIF-hosted Au deposits," is funded through the Targeted Geoscience Initiative-4 (TGI-4) program (Lode Gold project) and a Collaborative Research and Development project with funding from Agnico-Eagle Mines Ltd and Goldcorp Inc. with matching funds from NSERC. It is designed to address the issue of whether there is a particular type of BIF that potentially represents a favourable host for gold mineralization and, if this is the case, whether there is a specific geochemical hydrothermal footprint for BIF-hosted gold deposits (Dubé and Gosselin, 2007).

A study of the primary geochemical characteristics of Algoma-type BIF may help develop a vectoring tool from unaltered to altered- mineralized zones and establish the pre-mineralization composition of BIF to allow better characterization and understanding of the mineralizing processes and geochemical footprint of any hydrothermal system.

Samples from the Superior and Churchill provinces will be examined:

- Two BIF-hosted gold deposits located in the Superior Province will be investigated. The Musselwhite deposit (11.23 Mt proven/probable grading 6.34 g/t gold in 2011) (http://www.goldcorp.com/English/Investor-Resources/Reserves-and-Resources/default.aspx) (accessed April 8, 2013) is located in mafic to ultramafic volcanic rocks of the Eyapamikama Lake greenstone belt within the 3 to 2.9 Ga North Caribou terrane (Biczok et al., 2012). The McLeod-Cockshutt deposit (10 Mt produced grading at the end of the production at 4.04 g/t) (Macdonald, 1988) is located in the 2.7 Ga Beardmore-Geraldton greenstone belt in the Wabigoon Subprovince (Lafrance et al., 2004).

- The Churchill Province hosts the Meadowbank mine (24.5 Mt proven/probable ore reserves grading 2.8 g/t in 2011) (Agnico-Eagle Mines Ltd, 2012), and the Meliadine district (13 Mt proven/probable ore reserve grading 7.2 g/t in 2012) (http://www.agnicoeagle.com) deposits which occur in the 2.7 Ga Woodburn Lake Group. The deposits are hosted by mafic to felsic volcanic sequences with minor BIF (Ashton, 1985; Roddick et al., 1992; Aspler and Chiarenzelli, 1996).

This article presents the first geochemical results and focuses on data from the Meadowbank deposit area discovered in 1987 by Asamera Minerals Inc. (Armitage et al., 1996). Since then, several regional mapping programs (Henderson and Henderson, 1994; Zaleski et al., 1997a, b; Zaleski et al., 1999a, b; Sherlock et al., 2001a, b) and deposit scale studies (Armitage et al., 1996; Pehrsson et al., 2000, 2004; Sherlock et al., 2001a, b, 2004; Hrabi et al., 2003) have been conducted. A detailed study of the geological and hydrothermal footprint and structural setting of the Meadowbank deposit was undertaken in 2011 by the Geological Survey of Canada and Agnico-Eagle Mines Ltd. as part of the TGI-4 Lode Gold project (Castonguay et al., 2012; Janvier et al., 2013).

The deposit, located within the western Churchill Province (Fig. 1), occurs in polydeformed Algoma-type BIF. The area is underlain by the Neoarchean Woodburn Lake Group of the Rae Domain (Fig. 1,2) characterized by bimodal volcanism with minor metasedimentary rocks. The latter consists of iron-formation and clastic metasediments, all intruded by mafic to felsic plutonic rocks (Armitage et al., 1996; Pehrsson et al., 2000, 2004; Sherlock et al., 2001a, b, 2004; Hrabi et al., 2003).

The Meadowbank gold mine is composed of four zones (Fig. 3): the Third Portage, North Portage, Goose Island, and the Bay zones, hosted by the Central BIF consisting of strongly altered and deformed sulphide-bearing iron-formation (Sherlock et al., 2001a; Hrabi et al., 2003; Sherlock et al., 2004). Between 2000 and 2003, the Vault deposit, hosted by sericite-chlorite and silica-altered intermediate to felsic volcanic rocks (Hrabi et al., 2003; Sherlock et al., 2004), was found about 5 km north of the Central BIF.

Recently, somewhat lower grade BIF-hosted mineralization that flank the other zones and known as the Far West, West IF, East BIF, and Grizzly were identified through mapping, drilling, and geophysical campaigns.

This study presents new geochemical data on BIF at the Far West, West IF, Central BIF, East BIF and Grizzly zones. Moreover, the study seeks to identify similarities and/or differences between mineralized (i.e. Central BIF, and Grizzly) and apparently non-mineralized BIFs (i.e. Far West and West IF) based on geochemical signatures.

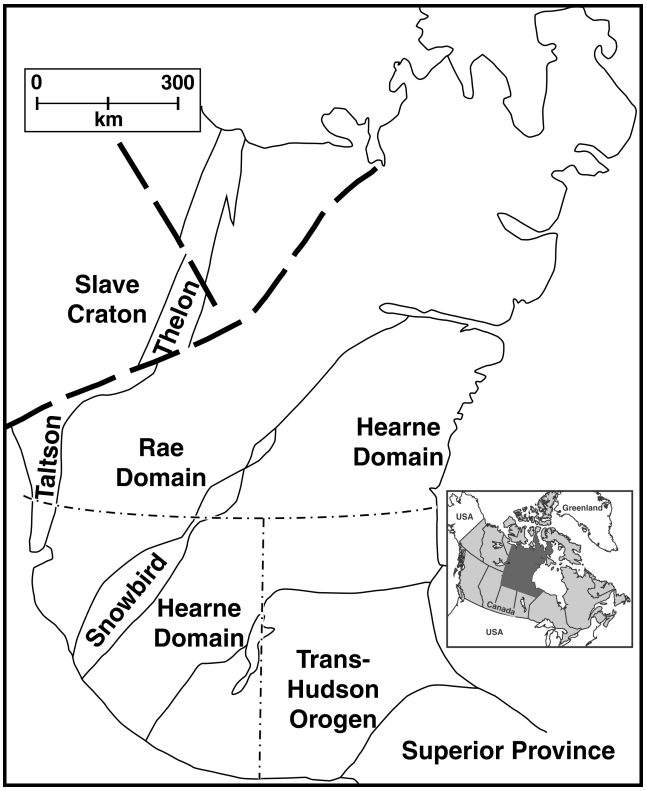

Figure 1. Map showing the Western Churchill Province divided into the Rae and the Hearne domains by the Snowbird tectonic zone and flanked by the Slave Craton (Eriksson et al., 2001)

GEOLOGICAL SETTING

Regional setting

The Archean Churchill Province has been subdivided by Hoffman (1989) into the Hearne and Rae domains, which are separated by the northeast-trending Snowbird Tectonic Zone (Fig. 1 and 2). The Hearne Domain is a juvenile, Neoarchean terrane flanked by the Paleoproterozoic Snowbird Tectonic Zone and the Trans-Hudson Orogen. It is a granite-greenstone terrane composed of multi-cyclic, mafic to felsic volcanic rocks intercalated with immature sandstones, pelites, and iron-formation; rare quartz arenites and spinifex-textured ultramafic rocks (Miller and Tella, 1995; Aspler and Chiarenzelli, 1996). The Rae Domain is a block bounded by the Paleoproterozoic Thelon Domain to the northwest, the Snowbird and New Quebec domains to the south, and the Torngat Orogen to the east. The block is composed of granitoids and mafic-ultramafic volcanic rocks, iron-formation, shallow-water quartz arenite and minor felsic volcanic rocks (Miller and Tella, 1995).

Miller and Tella (1995) recognized three lithostratigraphic sequences in the Rae Domain based on rock association and/or age of volcanism. Greenstone belts located north of the Snowbird Zone consist of the ca. 2.7 Ga Woodburn Lake Group (Ashton, 1985; Roddick et al., 1992;

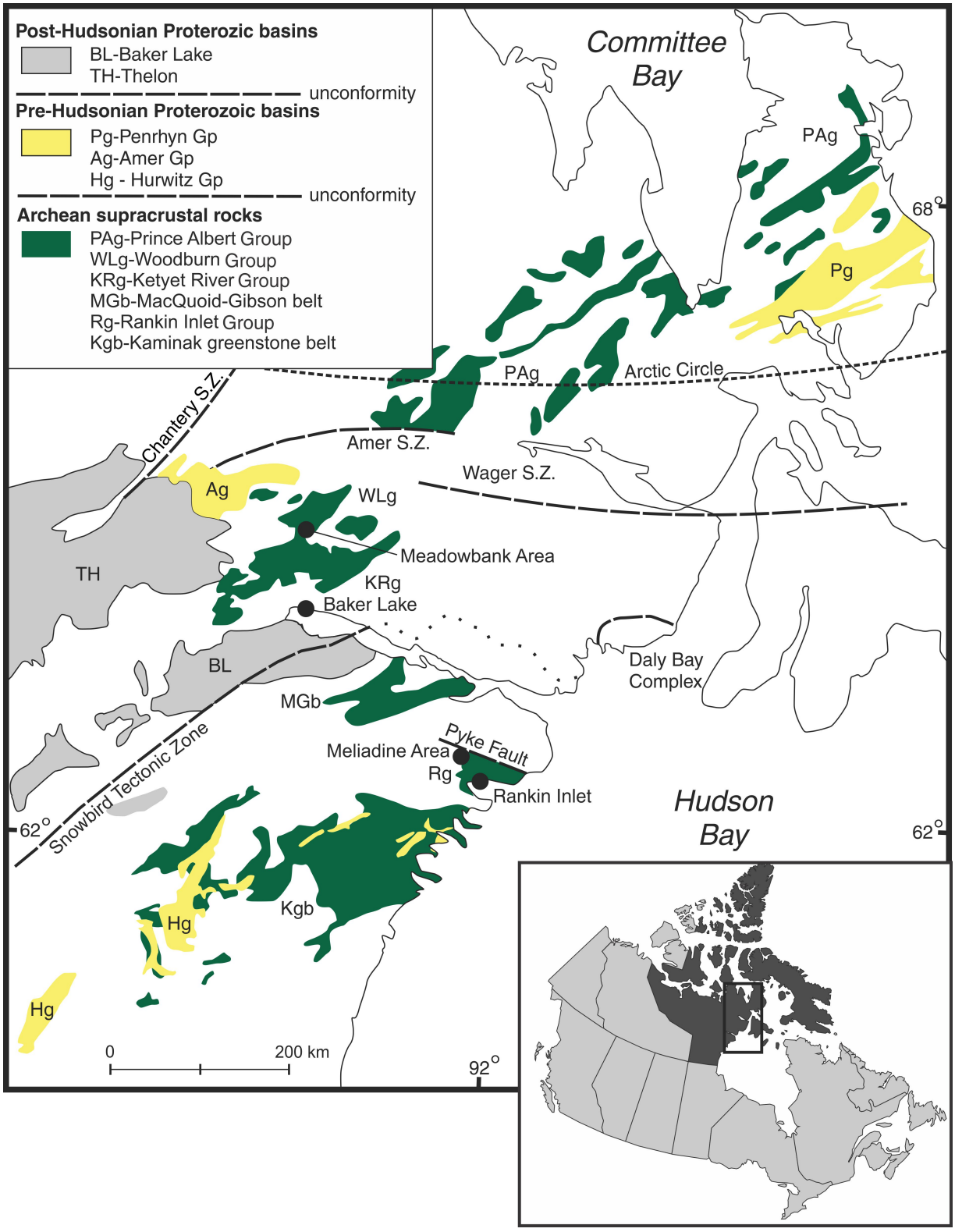

Figure 2. Simplified regional geological map of the Rae and Hearne domains (*from* Hrabi et al., 2003)

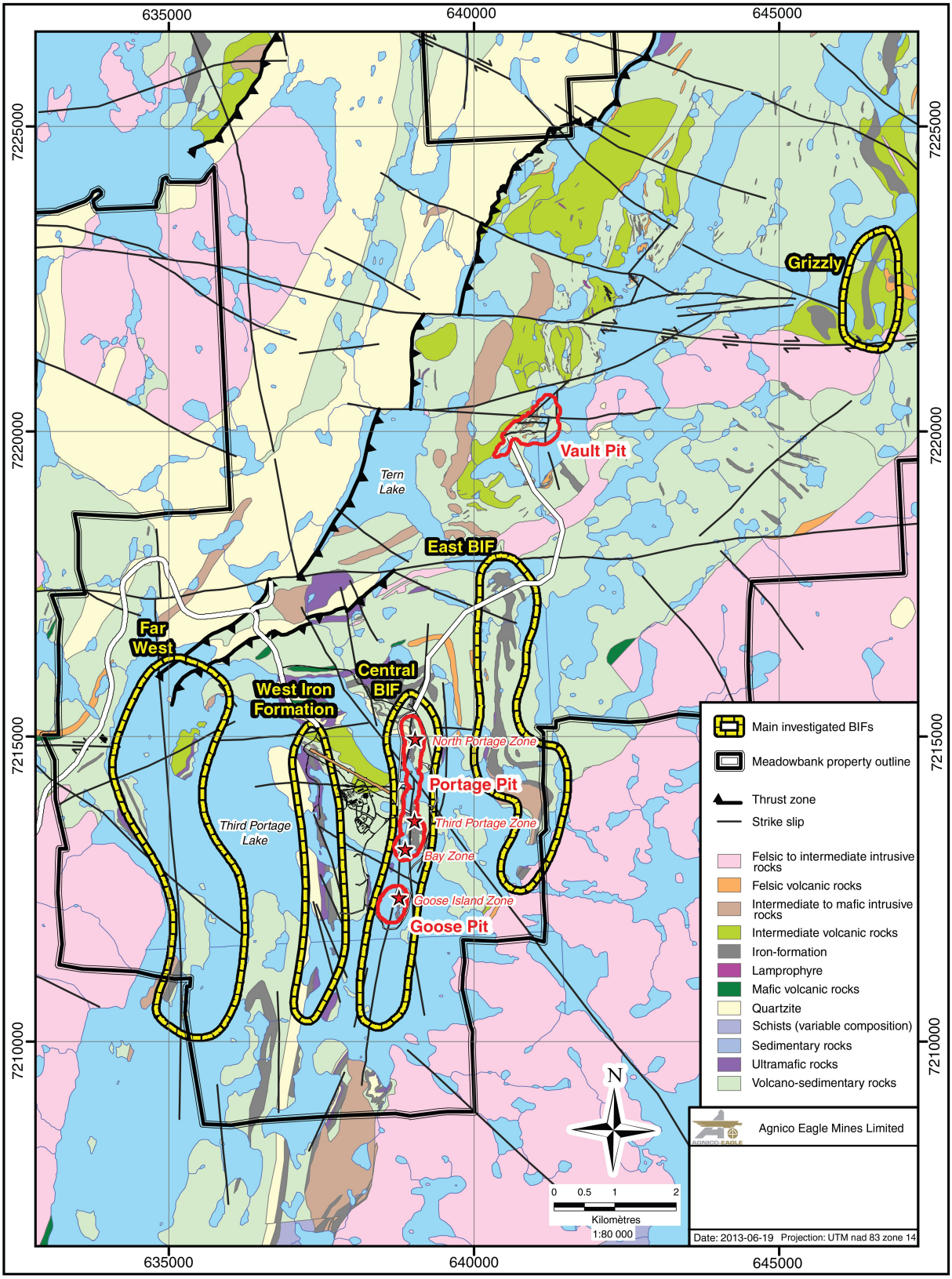

Figure 3. Main BIFs in Meadowbank area sampled for the project (*from* Agnico-Eagle Mines Ltd.)

Aspler and Chiarenzelli, 1996) and the ca. 2.9 Ga Prince Albert Group (Schau, 1982; Aspler and Chiarenzelli, 1996). The Rae Domain and the northern Hearne subdomain are characterized by the presence of widespread ca. 2.6 Ga granitoids and a poorly understood ca. 2.5 Ga metamorphism, which are absent in the central Hearne Domain.

In terms of depositional setting, Aspler and Chiarenzelli (1996) proposed that the continental supracrustal successions of the Rae Domain were deposited during extension of a continental basement block named 'Nunavutia' (Schau and Ashton, 1988) and were later overlain by volcanic rocks interpreted as a back-arc sequence or an arc-trench system.

Geologic setting of the Meadowbank deposit area

The Meadowbank deposit area is underlain by the Neoarchean Woodburn Lake Group of the Rae Domain, characterized by tholeiitic komatiitic, mafic and ultramafic metavolcanic rocks, with associated calc-alkaline felsic tuffs and flows intercalated with iron-formation, and wacke to mudstone metasedimentary rocks; these units are intruded by mafic to felsic plutonic rocks. The regional metamorphic grade ranges, going from north to south, from middle greenschist to amphibolite facies.

The Meadowbank area contains two main gold deposits: the Meadowbank mine and the Vault deposit. The Meadowbank mine is mainly hosted within strongly altered and deformed, sulphide-bearing portions of the Central BIF (Fig. 3; Sherlock et al., 2001a; Hrabi et al., 2003; Sherlock et al., 2004), whereas the Vault deposit is hosted by sericite-chlorite and silica-altered intermediate to felsic volcanic rocks (Hrabi et al., 2003; Sherlock et al., 2004). Since 2007, several smaller, lower grade mineralized zones have been the focus of exploration.

Volcanic rocks

The Woodburn Lake Group is a 2.74 to 2.71 Ga bimodal volcanic suite represented by felsic-intermediate volcanic rocks and ultramafic to mafic rocks (Davis and Zaleski, 1998; Zaleski et al., 2001). Their depositional setting consists of a partly subaqueous continental rift environment (Annesley, 1989).

Felsic-intermediate volcanic and volcaniclastic rocks

The 2.73 to 2.71 Ga felsic to intermediate (rhyolite-andesite) flows and fragmental rocks account for a significant portion of units in the Meadowbank area. (Davis and Zaleski, 1998; Zaleski et al., 2000; Sherlock et al., 2004). The major subunits are

- Massive felsic flows and subvolcanic intrusive rocks recognized to the east of the Meadowbank area in the structural footwall of the Third Portage Lake area deposits and hosting the Vault deposit. This unit has quartz and plagioclase phenocrysts in a fine-grained quartzofeldspathic matrix.
- Thin-bedded volcaniclastic rocks occur east and west of the massive felsic metavolcanic rocks and cover much of the Meadowbank deposit area. Beds are 1 to 5 cm thick with rare sedimentary structures, (Sherlock et al., 2001a, b; 2004). These beds have blue-grey quartz and feldspar grains in a matrix of epidote-biotite-chlorite-muscovite-sericite (Sherlock et al., 2001a, b; 2004). The rock is moderately to strongly foliated.
- Medium-bedded volcaniclastic rocks are commonly interbedded with the Central BIF in the Third Portage Lake area. Beds are 20 cm to 3 m thick. This subunit is mainly composed of quartz and feldspar grains within a biotite-epidote-muscovite-chlorite-sericite matrix with local blue-grey quartz phenocrysts (Sherlock et al., 2001a, b; 2004). The rock is strongly foliated and banded with occasional elongated potassium feldspar clasts (Sherlock et al., 2001a; 2004).

Ultramafic volcanic rocks

The rare ultramafic rocks in the Meadowbank area (Armitage et al., 1996) are strongly foliated and serpentinized, and primary textures, such as spinifex texture and pillows, are rarely preserved (Armitage et al., 1996). These rocks are blue-green, fine to medium grained and are composed of talc-amphibole-chlorite-carbonate and amphibole-chlorite-biotite assemblages, with notable variations in size and colour of the amphibole (Armitage et al., 1996; Sherlock et al., 2004).

Sedimentary rocks

The >2.62 Ga sedimentary package unconformably and/or structurally overlies the volcanic rocks and, in common with the volcanic package, it formed in a continental rift setting (Zaleski et al., 2000).

Banded iron-formation

Numerous continuous to discontinuous units of Algoma-type BIF ranging in thickness from 0.2 to 10 m have been identified. These BIFs include the Far West IF, West IF, Central BIF, East BIF, and Grizzly IF units all generally interlayered with the volcanic rocks and locally with a quartzite unit (Sherlock et al., 2001a, b; 2004) (Fig. 3).

The iron-formations display laminated magnetite and chert with associated layers (0.2 to 5 cm thick) of grunerite/biotite or cummingtonite/biotite or garnet/biotite observable with minor chlorite, muscovite, ankerite, siderite, stilpnomelane and apatite (Armitage et al., 1996; Hrabi et al., 2003; Sherlock et al., 2004). Previous workers have ascribed variations in the composition of amphibole to metamorphic processes (Armitage et al., 1996).

Discontinuous chlorite-rich bands (1 to 5 cm thick) locally interlayered with BIF may represent clastic sediments, a transition between chemical and clastic deposition (Armitage et al., 1996; Agnico-Eagle Mines Ltd, 2008), or volcanic detritus, suggestions requiring analytical confirmation.

The Central BIF is generally associated with intermediate volcanic rocks and ultramafic rocks. Due to variation in metamorphic grade, the Third Portage area (i.e. the larger mineralized BIF) is composed of cummingtonite and biotite assemblages; the middle part shows grunerite, biotite and minor garnet; and southward, Goose Island is composed of porphyroblastic garnet and biotite within the BIF. Mineralization is composed of pyrrhotite, pyrite, and sparse chalcopyrite and arsenopyrite. Pyrite also occurs as vuggy clusters in quartz veins and at the margins of quartz veins where it typically replaces pyrrhotite and magnetite (Armitage et al., 1996; Castonguay et al., 2012; Janvier et al., 2013).

In the mine vicinity, the non-mineralized East BIF is about 10 m thick and generally surrounded by intermediate volcanic rocks and locally by ultramafic rocks. This BIF is at middle greenschist facies and is characterized by well banded magnetite-quartz iron formation.

In the mine vicinity, the West BIF is surrounded by intermediate volcanic rocks and locally by quartzite and ultramafic rocks. The IF is about 10 m thick and is composed of pyrrhotite-rich cherty bands (2–10 modal %). Metamorphic grade ranges from upper greenschist to amphibolite and is characterized by a grunerite-, hornblende-, and stilpnomelane-bearing assemblage. Despite the presence of sulphides, the West IF did not return significant gold assays (<500 ppb) (Armitage et al., 1996; Agnico-Eagle, pers. comm., 2012).

The Far West BIF is surrounded by intermediate volcanic rocks, locally quartzite, and rarely some ultramafic rocks. It is about 10 m thick and dominated by pyrite. It is barren except for an interval of 3.6 m with an average of 2.81 g/t Au located in the north part. Gold mineralization seems to be associated with late, isolated pyrite veins (Agnico-Eagle, pers. comm., 2012).

The Grizzly BIF is surrounded by intermediate volcanic rocks and locally ultramafic rocks. In 2012, the zone was penetrated by 8 drillholes totaling 1909 m. This IF displays a different style of alteration with quartz flooding, ankerite, sericite, cummingtonite and visible gold. This alteration style is described here for the first time. The zone occurs near a body of younger massive granite.

Quartzite and associated sedimentary rocks

The quartzite forms a significant marker unit within the sedimentary rocks that unconformably overlie the volcanic rocks. Detrital zircons are ca. 2.81 Ga (Davis and Zaleski, 1998) along with a minimum age of 2.62 Ga (Zaleski et al., 2000). This unit forms massive to bedded intervals, mainly in the hanging wall of the deposit in the western part of the Meadowbank area along the West BIF (Zaleski et al., 2000; Sherlock et al., 2004), and is characterized by a strong foliation, defined by aligned muscovite and epidote grains (Zaleski et al., 2000; Sherlock et al., 2001a, b; Sherlock et al., 2004). An oligomictic conglomerate forms the basal part of the quartzite, ranging from 1 to 10 m thick, and containing quartz porphyry, granite, quartzite, quartz veins, and fine-grained sedimentary clasts. Locally, where not in fault contact, upward-graded beds provide a younging direction, which indicates that the quartzite stratigraphically overlies the ultramafic volcanic units (Zaleski et al., 2000; Sherlock et al., 2004).

Wacke to mudstone sedimentary rocks

At the south end of Tern Lake, medium to dark grey-brown-green wacke, wacke/siltstone, and mudstone units are interlayered with intermediate volcanic rocks and exhibit diffuse contacts. Grain size is highly variable within the wacke, and clasts consist of rounded quartz, feldspar, and lithic grains in a fine-grained quartz-feldspar-biotite-chlorite matrix (Sherlock et al., 2004). Locally, well preserved layering or bedding is present and a homogeneous clastic texture is noted.

The similarity in overall composition and the spatial association with intermediate volcanic rocks suggest that the sedimentary units may have been sourced from the intermediate volcanic rocks (Sherlock et al., 2004).

Intrusive rocks

Intrusive rocks in the Meadowbank area range from Archean to Paleoproterozoic in age.

Granite and granodiorite

Archean granitic bodies ranging from 2.62 to 2.59 Ga cut the supracrustal rocks (Davis and Zaleski, 1998). In the Tern Lake area, a northeast-trending porphyry is dated at ca. 2.63 Ga (Pehrsson et al., 2000). Archean granitic intrusive rocks are also present as minor granitic to syenitic stocks and dykes.

The Nueltin suite Paleoproterozoic granitoids, northwest and east of Third Portage Lake (to the east of the Vault deposit) intrude the volcanic unit. The granite is coarse grained, leucocratic, and shows vuggy textures (Pehrsson et al., 2000). Just east of the Vault Pit area, the granitic sills and dikes join to form an east-west-trending, fractured, variably chloritized intrusion (Agnico Eagle Mines Ltd, 2008).

Monzonite

In the northern part of the Meadowbank area, a weakly foliated, brown-grey monzonite unit consisting of fine- to medium-grained quartz, plagioclase, potassium feldspar and equigranular biotite occurs. Ca. 1.85 Ga thin dykes of red, biotite-hornblende syenite to quartz syenite cut the quartz monzonite and intermediate volcanic rocks (Tella et al., 2001).

Diorite to gabbro

To the east and west of Tern Lake and northeast of the Meadowbank area, weakly foliated, leucocratic diorite to gabbro bodies are recognized. They are characterized by a homogenous, medium-grained, ophitic and equigranular texture. Their alteration is characterized by fine- to medium- grained plagioclase and chloritized amphibole (Sherlock et al., 2001a, b; Sherlock et al., 2004).

Structural geology

The structural context of the Meadowbank area is complex, consisting of four regional-scale ductile deformation events spanning the Neoarchean to Paleoproterozoic (e.g. Henderson et al., 1991; Ashton, 1985). Two of these deformational events have had a significant effect on the geometry of the mineralized bodies in the Third Portage area (Ashton, 1985; Sherlock et al., 2004; Janvier et al., 2013). Some relict bedding (S0) is preserved in the quartz arenite and in iron-formation (Armitage et al., 1996).

D1 Deformation

Although Pehrsson et al. (2000) have defined a pre-D1 deformation; the most clearly recognized deformation is D1, associated with shallowly plunging, folds (F1), a penetrative fabric (S1), and lineations (L1). The D1 deformation event is Paleoproterozoic, bracketed between ca. 2.62 to 2.59 Ga and ca.1.835 Ga (Roddick et al., 1992; Pehrsson et al., 2000).

D2 Deformation

The D2 deformation is the main structural event in the Meadowbank area. It produced folds (F2), axial planar foliation (S2), strong lineations (L2) and west-directed reverse faults or shear zones (Pehrsson et al., 2000; Wilkinson et al., 2000). D2 structures are hosted in iron-formations in the central part of Central BIF (Armitage et al., 1996). The high-strain zone that hosts the Vault deposit is interpreted by Hrabi et al., (2003) to be related to D2 deformation. D2 is estimated at ca. 1.8 to 1.9 Ga (Pehrsson et al., 2000).

D3 Deformation

The D3 deformation is defined by shallowly plunging F3 folds and a crenulation lineation (L3) (Pehrsson et al., 2000). The expression of D3 is more prominent south of Third Portage Lake (Hrabi et al., 2003). F3 folds are defined by a southeast-verging minor fold set with shallowly to moderately northwest-dipping (<40°) axial surfaces (Pehrsson et al., 2000; Wilkinson et al., 2000; Sherlock et al., 2004). S3 foliation crenulates S2. The F3 folds reorient the S2-S1 intersection lineation in the iron-formation and are themselves folded by the northeast trending F4 axes (Pehrsson et al., 2000; Sherlock et al., 2004). An age of ca. 1.790 Ga for D3 deformation is suggested by Pehrsson et al., (2000).

D4 Deformation

The D4 deformation has an important effect on the geometry of units and the mineralized zones in the Meadowbank deposit area (Zaleski et al., 1997b; Sherlock et al., 2001b). It consists of folds (F4) with steeply dipping axial surfaces and local crenulation cleavages (S4). The type 2 (mushroom) fold interference pattern results from superposition of vertical F4 folds on inclined F2 folds (Pehrsson et al., 2000; Wilkinson et al., 2000; Sherlock et al., 2004). D4 affects the ore bodies, and is post mineralization. An age of ca. 1.835 to 1.760 Ga is estimated for D4 (Pehrsson et al., 2000; Wilkinson et al., 2000; Sherlock et al., 2004).

Metamorphism

Three distinct regional metamorphic events associated with structural events occurred in the Meadowbank area. The metamorphic grade varies from low to mid-greenschist to amphibolite facies.

The first event, M1, produced greenschist facies assemblages for which the pressure is unknown. Its association with S1 fabrics allows its timing to be constrained. Based on field observations, M1 predates the development of D2 deformation (ca. 1.8–1.9 Ga) and postdates the ca. 2.60 Ga granite suite.

The second event (M2) is defined by mid-greenschist- to amphibolite-facies assemblages (grade increasing southward) and is interpreted to be coeval with D2 deformation. The S2 fabrics at amphibolite grade are characterized by chloritoid, kyanite, chlorite, biotite, staurolite, andalusite,

and garnet. North of the Meadowbank area, mid-greenschist-facies conditions associated with the growth of kyanite in the quartzite unit and grunerite-chlorite in the BIF suggest a temperature near 400°C and pressure of at least 2.5 kbars (Armitage et al., 1996). The central part of the Meadowbank area is characterized by upper-greenschist-facies assemblages at a temperature of about 450°C at lower pressures. Finally, in the southern part of the Meadowbank area, in the Goose Island zone (Fig. 3), assemblages of biotite-staurolite-muscovite suggest temperatures near 550°C and a pressure at least 3.0 kbars.

A third event (M3) is defined by mid-upper greenschist- to amphibolite-facies assemblages. This event is characterized by the growth of a new generation of biotite, garnet, cummingtonite, and actinolite overprinting D2 structures and is contained in S3 fabrics. The mineral assemblage suggests a temperature near 450°C and a pressure of 3 kbars (Pehrsson et al., 2000). M3 is considered to be post-mineralization because of the overprinting of the ore zones by D3 structures. Sherlock et al., 2004 estimated an age of 1.8 Ga.

Mineralization

The setting and characteristics of gold mineralization have been documented within the Third Portage Lake area through government mapping and regional- and deposit-scale metallogenic studies (Roddick et al., 1992; Armitage et al., 1996; Davis and Zaleski, 1998; Kerswill et al., 1998, 2000; Kerswill, 2000; Pehrsson et al., 2000; Sherlock et al., 2001a, b; Pehrsson et al., 2004). These studies, coupled with exploration, have delineated four principal mineralized zones: the Third Portage, North Portage, Goose Island, and the Bay zone (Fig. 3). Most recently the Vault deposit (Hrabi et al., 2003), located about 5 km to the north-northeast of the principal deposits, has been delineated. The Vault deposit will not be discussed any further here.

The orebodies of the Meadowbank Mine consist of several subparallel bands of auriferous iron-formation, part of the Central BIF. Sherlock et al. (2001a, b) suggested that the orebodies are mostly developed at the contact between an ultramafic body and the volcanosedimentary package. According to Armitage et al., (1996) and Sherlock et al., (2001a, b), epigenetic gold mineralization is closely associated with D1-D2 deformation and originated from the circulation of metasomatic fluids, enriched in Mg, K, Ca, S, As, Cu, and Au.

At the northern end of the Central BIF, in the North Portage Zone, weak mineralization and alteration occur (Armitage et al., 1996). An assemblage of grunerite, hornblende, and stilpnomelane typical of the mid-greenschist facies affects this zone. Fibrous needles of grunerite grow across the magnetite-chert interface. The mineralization is associated with disseminated pyrrhotite, pyrite, chalcopyrite, and arsenopyrite. Pyrrhotite forms fine-grained clusters and discontinuous, layer-parallel veinlets in grunerite-bearing magnetite-rich bands of BIF (Armitage et al., 1996). Pyrite replaces pyrrhotite and magnetite and chalcopyrite/arsenopyrite are present in the form of inclusions in pyrrhotite. The North Portage mineralization is similar to the mineralization hosted in the West BIF (Fig. 3).

The Third Portage Zone contains the greatest amount of mineralization (10.59 Mt proven/probable grading 2.98 g/t gold in 2011; Agnico Eagle Mines Ltd, 2012). An assemblage of fine-grained cummingtonite, minor fine- to medium-grained chlorite and biotite is interpreted to be related to upper-greenschist-facies metamorphism. According to Armitage et al. (1996) the cummingtonite grew in the same manner as the grunerite at mid-greenschist facies (i.e. at the interface between magnetite and chert bands). A similar mineralogical assemblage is present in the north (i.e. pyrrhotite-pyrite-chalcopyrite-arsenopyrite), but the pyrrhotite is more concentrated here as massive to disseminated grains and as pervasive replacement of magnetite. Chalcopyrite and arsenopyrite are present as inclusions in pyrrhotite.

ANALYTICAL METHODS

Thirty-nine samples of iron-formation were collected for petrographic analysis from drill core and outcrops in the Far West, West IF, Central BIF, East BIF, and Grizzly areas (Fig. 3). Chert or chert-carbonate phases of each sample were studied in preparation for geochemical analysis. Emphasis was placed on collecting samples representing the top, middle, and base of BIF units. An effort was also made to avoid BIF with chert bands <0.05 cm in thickness, as analysis of bands of this thickness is difficult. Chert bands were analyzed in preference to Fe-rich bands to minimize the effects of diagenetic alteration. Thin sections prepared from these samples were examined in detail using transmitted- and reflected-light microscopy and the SEM-EDS.

Trace-element and REE geochemistry were obtained on 100 µm thick polished sections following petrographic study. Based on the latter, areas for analysis were selected to minimize the presence of phases other than quartz after chert, alteration, and inclusions. Analyses were made using a Resonectics Resolution M-50 laser ablation instrument coupled to a Thermo X-Series II quadrupole ICP-MS at the Geochemical Fingerprinting Laboratory of Laurentian University, in Sudbury, Ontario. The protocol used follows that in Kamber and Webb (2007). Traverses, rather than spot analyses, were made on the preselected areas using 140 and 190 µm beam diameters with a repetition rate of 10 Hz and an energy density of 7 J/cm^2. Samples were analyzed for the 14 REEs in addition to Li, Be, Sc, Ti, V, Cr, Co, Ni, Cu, Zn, Ga, As, Rb, Sr, Y, Nb, Mo, Ag, Cd, In, Sn, Sb, Cs, Ba, Hf, Ta, W, Tl, Pb, Th, U, and Au. Silicon was used as the internal standard and the NIST 612 glass standard was analyzed at the beginning and at the end of each traverse.

Only the data from samples for which data for all the REEs were above the detection limit are discussed. Also, for this study, the Queensland (MUQ) shale standard was used to normalize samples for REE+Y studies. This shale standard is commonly used for normalization of Archean BIF data due to its dominantly mafic volcanic provenance that is similar to an average terrigenous input into the ocean from weathering of upper continental crust (e.g. Bolhar et al., 2005; Thurston et al., 2012).

Review of REE+Y systematics in BIF

The abundance of REE+Y in chert is controlled by three possible processes: 1) precipitation from open marine seawater (e.g. Bau and Dulski, 1996); 2) precipitation from hydrothermal (i.e. vent sourced) fluids (e.g. Allwood et al., 2010; Danielson et al., 1992); and 3) replacement processes (e.g. Hanor and Duchac, 1990). All of these can be influenced by terrigenous input (Alexander et al., 2008) and oceanographic processes, such as precipitation of phosphates. In the literature it is customary to normalize samples using a shale standard to minimize the influence of any terrigenous input due to the weathering of the upper continental crust. Yttrium is a rare-earth element with a valence of +3, though not a lanthanide, thus it is inserted into the conventional rare-earth diagram between Dy and Ho. Given the large beam size, if other phases were present they would affect the REE+Y pattern and values for elements such as Ga (clay mineral contamination), Zr (felsic ash contamination), and Th/U (phosphate contamination) and thus this must be monitored for.

In a modern setting, the shale-normalized REE+Y pattern for material precipitated from seawater (Fig. 4) shows:

a) depletion in light rare-earth elements (LREEs) relative to heavy rare-earth elements (HREEs);

b) a strongly super-chondritic Y/Ho ratio which produces a positive Y anomaly (Y/Ho >27 and often between 40 and 90);

c) positive La anomaly (La/La* between 1.15 and 1.3);

d) positive Gd anomaly (Gd/Gd* between 1.3 and 1.5);

e) a well developed, negative Ce anomaly resulting from the oxidation of Ce^{+3} to Ce^{+4} in the water column; and

f) minor positive Lu anomalies where analyses of Lu at appropriate levels are available.

Due to the anoxic character of Archean seawater, the shale-normalized REE+Y patterns for Archean seawater are very similar to modern seawater except that Ce shows a negative anomaly (Planavsky et al., 2010).

Based on the above, samples with an Archean seawater pattern should be characterized by the following when normalized to shale in the REE plots:

a) depletion in LREEs relative to middle and heavy REEs;

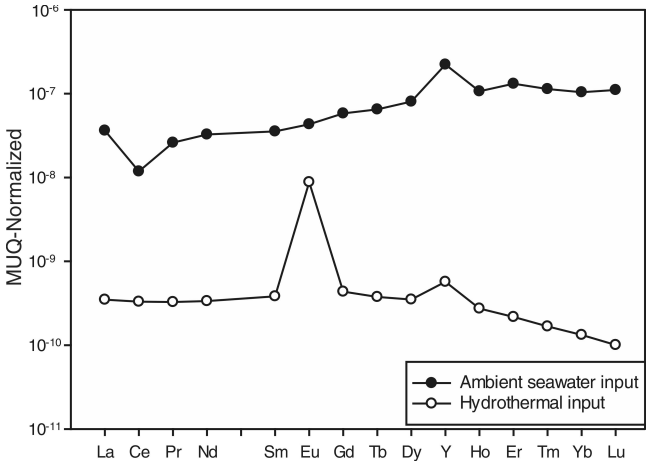

Figure 4. REE patterns illustrating modern settings ambient seawater input and hydrothermal input (after Bau and Dulski, 1996)

b) a strongly super-chondritic Y/Ho ratio (Y/Ho between 50 and 65);

c) positive La and Gd anomalies (0.3 to 0.5 and 0.15 to 0.3, respectively); and

d) variable, but well developed, positive Eu anomalies (Kamber et al., 2004).

Positive La, Y, and Gd anomalies indicate precipitation from seawater (Fig. 4) under anoxic conditions (absence of negative Ce anomaly) in oceans influenced by high-temperature (>250°C) hydrothermal fluids (Fig. 4) (i.e. positive Eu anomaly: Kamber et al., 2004).

Hydrothermal precipitates are characterized by a lack of LREE depletion, La and Gd anomalies, and the presence of a variably intense Eu anomaly. Crustal contamination may include single mineral phases such as phosphates, clays, and/or resistant minerals (e.g. zircon, xenotime etc.), which bring about a range of effects upon the REE+Y patterns. Given the range of effects, they are not illustrated here.

The precipitation of iron oxy-hydroxides will decrease the abundance of LREEs with increasing water depth ((Kamber, 2010).

Results

Samples from Far West, West IF, Central BIF, East IF, and Grizzly were normalized to the Queensland (MUQ) shale standard. Despite minor exceptions, REE+Y normalized data presented in tables (Table 1, 2, 3, 4) and diagrams (Fig. 5) show relatively uniform REE+Y patterns. The data include a moderate enrichment in HREEs relative to LREEs and MREEs (Nd/Yb_{MUQ} = 0.1–0.6) and Gd, Eu, and Y display distinct positive anomalies (Gd/Gd^*_{MUQ} = 0.9–1.3; Eu/Eu^*_{MUQ} = 1.2–5.1; Y/Y^*_{MUQ} = 0.8–1.9), La anomalies are calculated following the procedure of Lawrence and Kamber (2005) using extrapolated Pr and Nd values (La/La^*_{MUQ} = 0.8–4.6).

Table 1. Abundances of REE+Y and selected elements (in ppm) for samples from the Central BIF.

Central BIF									
Source file	**AMB-126222**	**AMB-126223**	**AMB-126224**	**AMB-126225**	**AMB-126226**	**AMB-126227**	**AMB-126230**	**AMB-126231**	**AMB-126232**
La	0.020	0.047	0.054	0.023	0.004	0.007	0.003	0.071	0.031
Ce	0.015	0.049	0.039	0.019	0.004	0.006	0.005	0.068	0.024
Pr	0.015	0.047	0.034	0.017	0.004	0.006	0.006	0.073	0.021
Nd	0.028	0.058	0.036	0.019	0.004	0.007	0.008	0.081	0.022
Sm	0.029	0.088	0.039	0.025	0.005	0.008	0.013	0.189	0.014
Eu	0.135	0.204	0.117	0.063	0.024	0.027	0.022	0.353	0.038
Gd	0.068	0.203	0.066	0.052	0.008	0.012	0.023	0.293	0.009
Tb	0.072	0.273	0.072	0.056	0.010	0.014	0.027	0.357	0.007
Dy	0.091	0.364	0.082	0.069	0.011	0.015	0.032	0.407	0.005
Y	0.237	0.495	0.123	0.152	0.016	0.022	0.042	0.367	0.006
Ho	0.116	0.402	0.091	0.085	0.014	0.017	0.035	0.400	0.005
Er	0.126	0.434	0.105	0.088	0.013	0.018	0.037	0.440	0.004
Tm	0.116	0.421	0.107	0.085	0.013	0.019	0.037	0.460	0.005
Yb	0.110	0.431	0.104	0.077	0.012	0.019	0.034	0.488	0.003
Lu	0.124	0.434	0.128	0.089	0.018	0.020	0.036	0.536	0.005
Th/U	0.881	1.312	0.128	0.780	0.154	0.565	0.134	1.218	2.028
Ni/Cr	1.941	1.597	2.545	0.643	0.859	0.900	1.051	0.036	0.833
Eu/Eu*	3.327	1.553	2.366	1.883	3.511	2.652	1.249	1.490	3.280
Pr/Yb	0.135	0.110	0.324	0.214	0.302	0.335	0.172	0.149	7.066
Y/Ho	2.039	1.230	1.349	1.791	1.204	1.290	1.210	0.919	1.059
La/La*	4.648	1.494	1.819	1.875	0.887	1.265	0.954	1.215	1.508
Ce/Ce*	1.860	1.273	1.234	1.371	0.945	1.132	1.134	1.045	1.132
Gd/Gd*	1.246	1.065	1.088	1.166	0.987	1.002	1.055	1.001	1.011
Pr/Sm	0.514	0.538	0.867	0.669	0.731	0.765	0.440	0.385	1.559
Zr	0.153	104.900	0.205	8.800	0.233	0.146	0.199	183.000	2.250
Th	0.006	1.220	0.005	0.035	0.002	0.012	0.003	7.700	0.043
U	0.007	0.930	0.043	0.045	0.012	0.021	0.023	6.320	0.021
Zr/U	23.499	112.796	4.801	197.309	19.915	7.053	8.690	28.956	106.132
Nd/Yb	0.254	0.135	0.348	0.249	0.290	0.369	0.222	0.166	7.191
Y/Y*	1.956	1.184	1.253	1.758	1.214	1.242	1.180	0.875	1.175

Table 2. Abundances of REE+Y and selected elements (in ppm) for samples from the East BIF.

	East BIF								
Samples	**AMB-126241**	**AMB-126242**	**AMB-126243**	**AMB-126245**	**AMB-126246**	**AMB-126247**	**AMB-126248**	**AMB-126249**	**AMB-126250**
La	0.182	0.005	0.062	0.004	0.002	0.003	0.002	0.012	0.005
Ce	0.149	0.007	0.054	0.004	0.002	0.004	0.002	0.014	0.006
Pr	0.169	0.009	0.055	0.004	0.002	0.005	0.002	0.014	0.007
Nd	0.186	0.013	0.057	0.006	0.002	0.007	0.003	0.021	0.009
Sm	0.214	0.021	0.055	0.009	0.003	0.016	0.006	0.030	0.015
Eu	0.518	0.119	0.192	0.024	0.010	0.062	0.028	0.132	0.097
Gd	0.270	0.035	0.081	0.014	0.005	0.023	0.010	0.055	0.025
Tb	0.275	0.039	0.083	0.014	0.006	0.023	0.011	0.057	0.027
Dy	0.326	0.051	0.108	0.015	0.006	0.026	0.013	0.059	0.031
Y	0.492	0.071	0.125	0.019	0.009	0.035	0.025	0.087	0.053
Ho	0.353	0.057	0.116	0.015	0.009	0.028	0.016	0.063	0.034
Er	0.389	0.069	0.137	0.016	0.008	0.028	0.016	0.068	0.038
Tm	0.378	0.077	0.151	0.018	0.013	0.031	0.020	0.063	0.036
Yb	0.385	0.090	0.172	0.017	0.011	0.032	0.019	0.064	0.038
Lu	0.420	0.120	0.194	0.020	0.015	0.041	0.026	0.080	0.048
Th/U	0.196	0.567	0.100	0.317	0.522	0.291	0.420	0.337	0.301
Ni/Cr	0.164	0.451	0.419	0.474	0.737	0.473	0.537	0.385	0.370
Eu/Eu*	2.198	4.359	2.949	2.292	2.672	3.272	3.833	3.449	5.122
Pr/Yb	0.439	0.104	0.320	0.251	0.169	0.160	0.125	0.224	0.179
Y/Ho	1.394	1.246	1.079	1.234	0.978	1.251	1.561	1.379	1.527
La/La*	1.312	1.025	1.213	1.706	1.237	1.408	1.431	1.773	1.272
Ce/Ce*	0.973	1.027	1.024	1.197	0.956	1.132	1.317	1.407	1.252
Gd/Gd*	1.055	1.066	1.085	1.141	0.998	1.075	1.068	1.154	1.094
Pr/Sm	0.791	0.434	0.993	0.503	0.640	0.320	0.419	0.485	0.449
Zr	2.170	0.461	0.970	0.550	0.860	0.224	1.120	0.178	0.425
Th	0.050	0.009	0.021	0.013	0.014	0.002	0.003	0.001	0.003
U	0.255	0.015	0.212	0.040	0.027	0.006	0.006	0.004	0.011
Zr/U	8.510	30.733	4.575	13.854	31.852	37.458	172.840	43.204	40.208
Nd/Yb	0.484	0.142	0.332	0.328	0.178	0.233	0.170	0.325	0.243
Y/Y*	1.325	1.128	0.988	1.202	1.009	1.245	1.531	1.325	1.458

Table 3. Abundances of REE+Y and selected elements (in ppm) for samples from the West IF.

	West IF							
Samples	AMB-126233	AMB-126234	AMB-126235	AMB-128328	AMB-128329	AMB-128330	AMB-128331	AMB-128332
La	0.014	0.003	0.011	0.003	0.128	0.239	3.273	1.019
Ce	0.013	0.004	0.010	0.003	0.066	0.229	2.910	0.805
Pr	0.013	0.005	0.011	0.003	0.057	0.219	2.242	0.684
Nd	0.016	0.007	0.015	0.003	0.063	0.239	2.312	0.787
Sm	0.025	0.023	0.018	0.004	0.056	0.217	2.293	0.665
Eu	0.056	0.142	0.088	0.017	0.217	0.260	3.180	0.832
Gd	0.048	0.060	0.026	0.010	0.077	0.173	3.288	0.796
Tb	0.047	0.085	0.026	0.015	0.068	0.154	3.515	0.699
Dy	0.053	0.095	0.030	0.025	0.075	0.149	4.689	0.828
Y	0.094	0.153	0.062	0.054	0.151	0.131	6.629	1.069
Ho	0.064	0.122	0.036	0.035	0.086	0.133	5.592	1.032
Er	0.073	0.137	0.042	0.049	0.098	0.117	6.149	1.204
Tm	0.073	0.153	0.048	0.062	0.096	0.110	5.519	1.442
Yb	0.076	0.151	0.057	0.071	0.108	0.110	4.713	1.446
Lu	0.097	0.190	0.070	0.078	0.139	0.115	3.916	1.412
Th/U	0.088	0.252	0.360	2.637	0.213	2.269	1.567	2.019
Ni/Cr	2.548	0.043	1.000	0.512	0.777	1.128	0.265	0.535
Eu/Eu*	1.745	3.916	4.203	2.558	3.516	1.318	1.215	1.226
Pr/Yb	0.170	0.031	0.199	0.036	0.530	1.993	0.476	0.473
Y/Ho	1.461	1.248	1.732	1.524	1.750	0.988	1.185	1.036
La/La*	1.701	1.895	1.857	1.541	2.689	1.304	1.552	1.972
Ce/Ce*	1.215	1.226	1.144	1.523	1.254	1.144	1.338	1.353
Gd/Gd*	1.237	1.062	1.087	0.932	1.180	0.980	1.091	1.153
Pr/Sm	0.513	0.206	0.629	0.596	1.014	1.009	0.978	1.029
Zr	5.800	0.111	0.790	0.319	0.300	19.100	43.400	20.100
Th	0.004	0.002	0.006	0.007	0.003	1.055	3.400	4.200
U	0.043	0.007	0.017	0.003	0.014	0.465	2.170	2.080
Zr/U	136.150	15.226	45.402	114.748	21.429	41.075	20.000	9.663
Nd/Yb	0.209	0.049	0.269	0.042	0.581	2.177	0.491	0.544
Y/Y*	1.368	1.179	1.596	1.273	1.643	1.052	1.129	0.956

Table 4. Abundances of REE+Y and selected elements for samples (in ppm) from the Far west and Grizzly BIFs.

	Far West			Grizzly	
Samples	AMB-126236	AMB-126238	AMB-126239	AMB-128334	AMB-128335
La	0.010	0.056	0.024	0.033	0.015
Ce	0.010	0.055	0.033	0.027	0.014
Pr	0.011	0.049	0.026	0.025	0.016
Nd	0.013	0.047	0.037	0.027	0.021
Sm	0.023	0.034	0.057	0.042	0.037
Eu	0.035	0.024	0.050	0.247	0.123
Gd	0.050	0.023	0.078	0.094	0.082
Tb	0.058	0.013	0.067	0.127	0.097
Dy	0.077	0.008	0.063	0.191	0.123
Y	0.159	0.007	0.075	0.322	0.189
Ho	0.110	0.007	0.058	0.242	0.139
Er	0.164	0.005	0.057	0.305	0.152
Tm	0.204	0.006	0.061	0.335	0.147
Yb	0.233	0.004	0.064	0.368	0.141
Lu	0.326	0.005	0.076	0.383	0.142
Th/U	0.143	0.406	0.281	0.080	0.054
Ni/Cr	0.530	0.761	0.729	1.779	1.989
Eu/Eu*	1.082	0.931	0.813	3.964	2.329
Pr/Yb	0.049	11.898	0.412	0.068	0.113
Y/Ho	1.452	1.079	1.304	1.329	1.361
La/La*	1.156	1.063	1.794	1.618	1.650
Ce/Ce*	0.982	1.082	1.746	1.200	1.129
Gd/Gd*	1.126	1.218	1.197	1.045	1.134
Pr/Sm	0.492	1.461	0.464	0.595	0.430
Zr	0.500	0.530	16.000	17.300	48.300
Th	0.004	0.023	0.055	0.014	0.007
U	0.029	0.056	0.196	0.176	0.123
Zr/U	17.241	9.447	81.633	98.295	392.683
Nd/Yb	0.057	11.459	0.584	0.075	0.149
Y/Y*	1.163	1.218	1.317	1.178	1.303

Due to the low concentrations of REE+Y, Y/Ho ratios are weakly positive, but were not used in this study. The positive La, Gd, and Y anomalies illustrate an ambient seawater influence, as explained previously.

The positive Eu anomaly is a common feature in rocks precipitated from Archean seawater modified by hydrothermal fluids (i.e. >250°C). The Nd/Yb_{MUQ} ratios could be associated with a Eu anomaly as a proxy for hydrothermal input or as terrigenous input (Bolhar et al., 2005).

Considering each BIF individually, some differences are apparent. Data for Far West (Fig. 5a) shows very erratic REE+Y patterns due to the very low abundance of REEs in chert bands and possible reworking of material by subsequent processes. This BIF will not be discussed further here, but may be resampled in the future to try to improve these results.

The West IF (Fig. 5b) data show fairly flat REE+Y patterns relative to other BIF with two distinct groups of samples present:

a) Samples AMB-126233, AMB-126234, AMB-126235, AMB-128328, and AMB-128329 show enrichment in HREEs relative to MREEs and LREEs (Nd/Yb_{MUQ} = 0.04–0.5), and positive Gd, La, Y, and Eu anomalies (Gd/Gd^*_{MUQ} = 0.9–1.2, La/La^*_{MUQ} = 1.5–2.6, Y/Y^*_{MUQ} = 1.1–1.6, and Eu/Eu^*_{MUQ} = 1.7–3.5) (Fig. 6a);

b) Samples AMB-128330, AMB-128331, and AMB-128332 show only a variable enrichment in HREE relative to MREE and LREE (Nd/Yb_{MUQ} = 0.4–2), and weak positive La and Eu (La/La^*_{MUQ} = 1.3–1.9, Eu/Eu^*_{MUQ} = 1.2–1.3) anomalies along with an absence of Gd and Y anomalies (Gd/Gd^*_{MUQ} = 0.9–1.1, Y/Y^*_{MUQ} = 0.9–1.1) (Fig. 6b).

The relatively flat patterns observed could be explained by crustal contamination and/or the presence of disseminated subhedral phosphate grains (i.e. fluorapatite) in the chert bands (Fig. 6b). The presence of crustal contamination is generally reflected by a relationship between $(Pr/Sm)_{MUQ}$ and Th and Ga, as the latter substitutes for Al and may be enriched in clay minerals of continental provenance (Bolhar et al., 2005). The source and origin of phosphate contamination has yet to be established. In general, phosphate contamination in BIF is not significant (Thurston et al., 2012; Bau and Alexander 2009).

Generally, the Archean shales and volcanic tuffs do not display significant positive Eu anomalies, as illustrated by the West IF data. Meanwhile, fluorapatite grains are present in each BIF and their shape could suggest a detrital origin representing part of the crustal contamination input. Theoretically, because of its presence in each BIF in the area, fluorapatite contamination should affect each BIF, producing a slightly concave-downward REE+Y pattern associated with a negative Eu anomaly (Fig. 6b) (after Sano et al., 2002).

Based on Pr/Sm_{MUQ} ratios, the Ga, Th, and Sr content and a REE+Y pattern similar to apatite (except for a negative Eu anomaly), the data suggest samples AMB-128330, AMB-128331, and AMB-128332 may represent phosphate contamination (Fig. 6c, d, e) (*after* Sano et al., 2002). This pattern suggests an association of these elements with terrigenous input (i.e. due to high concentration of Ga and Th) composed of phosphate and aluminum with a hydrothermal input explained by the positive Eu anomaly. In the traverse-based sampling method used, the laser could have encountered phosphates only in these three samples.

The Central BIF (Fig. 5c) data show relatively constant REE+Y patterns with enrichment in HREEs relative to MREEs (Nd/Yb_{MUQ} = 0.1–0.3) and positive Gd, La, Y and Eu anomalies (Gd/Gd^*_{MUQ} = 0.9–1.2, La/La^*_{MUQ} = 0.8–4.6, Y/Y^*_{MUQ} = 0.8–1.9 and Eu/Eu^*_{MUQ} = 1.5–3.5) that illustrate both ambient seawater and a hydrothermal input (Fig. 7a), except for one sample which shows an enrichment in LREEs

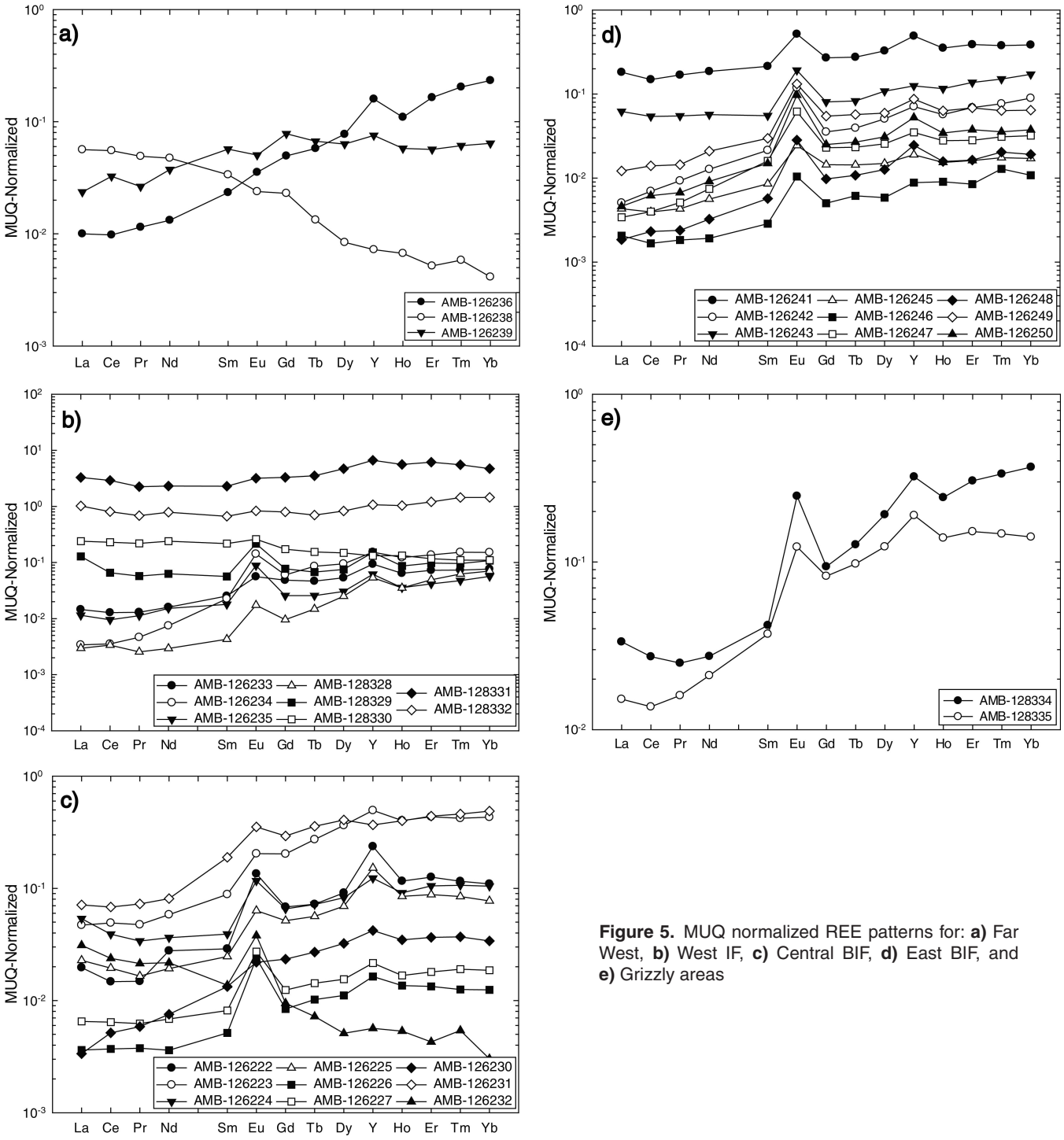

Figure 5. MUQ normalized REE patterns for: **a)** Far West, **b)** West IF, **c)** Central BIF, **d)** East BIF, and **e)** Grizzly areas

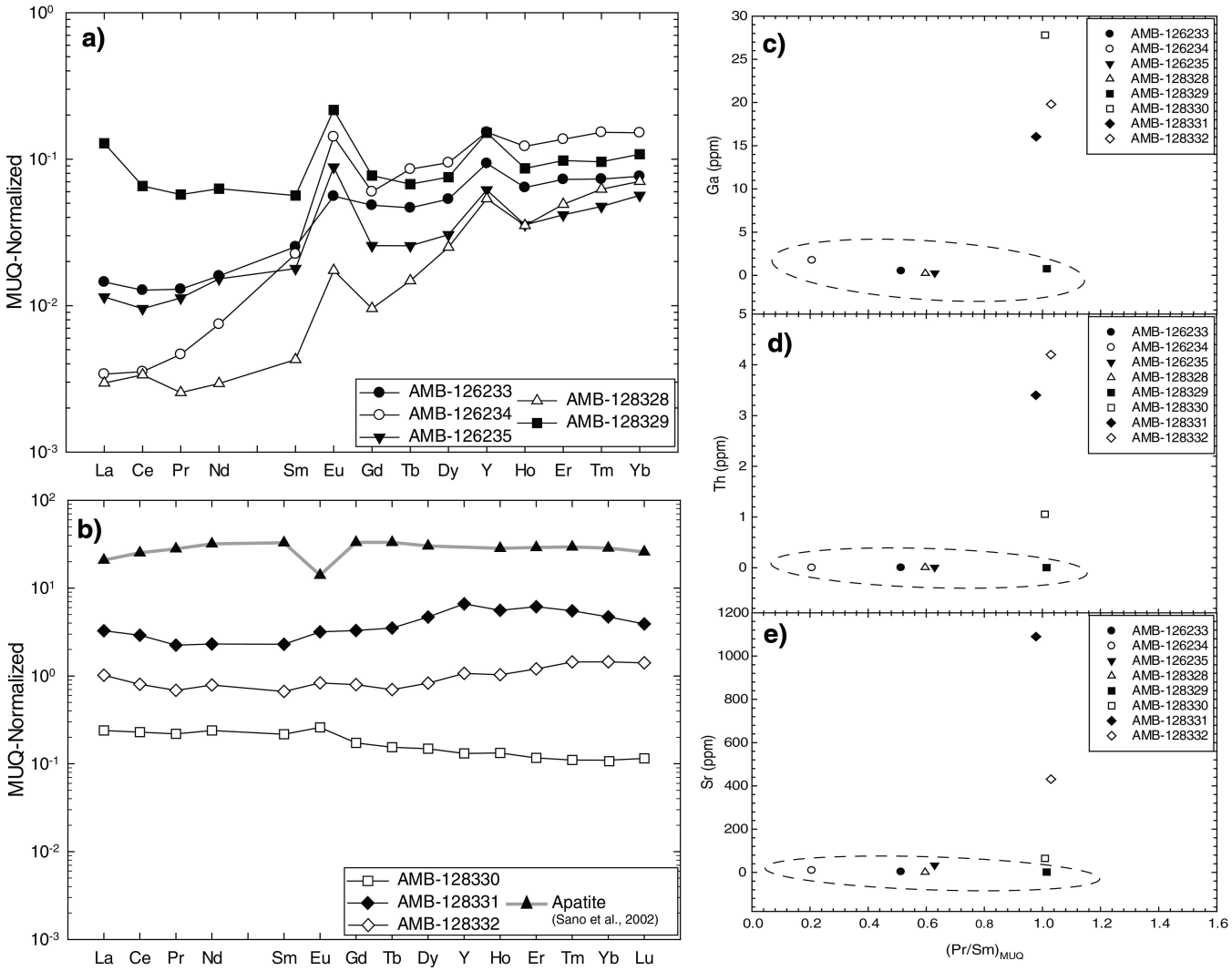

Figure 6. MUQ-normalized REE patterns for the West IF partition showing **a)** ambient seawater and hydrothermal input, and **b)** atypical REE+Y showing contamination; **c)** Ga vs. Pr/Sm_{MUQ}; **d)** Th vs. Pr/Sm_{MUQ}; **e)** Sr vs. Pr/Sm_{MUQ}.

relative to HREEs (Nd/Yb_{MUQ} = 7) (Fig. 7c) and a positive Eu anomaly (Eu/Eu^*_{MUQ} = 3.2). This spectrum, corresponding to sample AMB-126232, shows a very similar pattern to that of a garnet-quartz-envelope in the giant Broken Hill Zn-Pb complex (Spry et al., 2007), which is shown in Figure 7c for reference. Sample AMB-126232 also shows a strong correlation between $(Eu/Eu^*)_{MUQ}$ (i.e. proxy of calcium) and $(Pr/Sm)_{MUQ}$ (Fig. 7f), as well as Ga and $(Pr/Sm)_{MUQ}$ (Fig. 7d), which suggests the influence of garnet on the pattern. This artifact could be explained by the presence of a massive band of euhedral garnets that occurs very close to the traverse and which may have influenced the chert chemistry.

Additionally, samples AMB-126223 and samples AMB-126231(Fig. 7b) show an enrichment in Ga and Th relative to $(Pr/Sm)_{MUQ}$ ratios (Fig. 7d, e), which suggests crustal contamination.

The East BIF (Fig. 5d) data show a very consistent compositional range with enrichment in HREEs relative to MREEs (Nd/Yb_{MUQ} = 0.1–0.4) and positive Gd, La, Y, and Eu anomalies (Gd/Gd^*_{MUQ} = 0.9–1.1, La/La^*_{MUQ} = 1–1.7, Y/Y^*_{MUQ} = 0.9–1.4 and Eu/Eu^*_{MUQ} = 2.1–5.1) which suggests an ambient seawater and strong hydrothermal inputs (Fig. 8a).

In detail, however, samples AMB-126241, AMB-126243, and AMB-126246 show relatively flatter patterns (Fig. 8a) which are similar to apatite (after Sano et al., 2002), but lacking a negative Eu anomaly. The contents of Ga, Th, and Sr relative to $(Pr/Sm)_{MUQ}$ (Fig. 8c, d, e) illustrate a correlation between these elements; therefore, these results could be explained by some terrigenous input, similar to the West IF, with the laser traverses potentially having analyzed some grains of fluorapatite. Limited comparison shows a flat MUQ-normalized pattern for apatite; therefore, we do not expect a major effect from incorporation of minor amounts of fluorapatite.

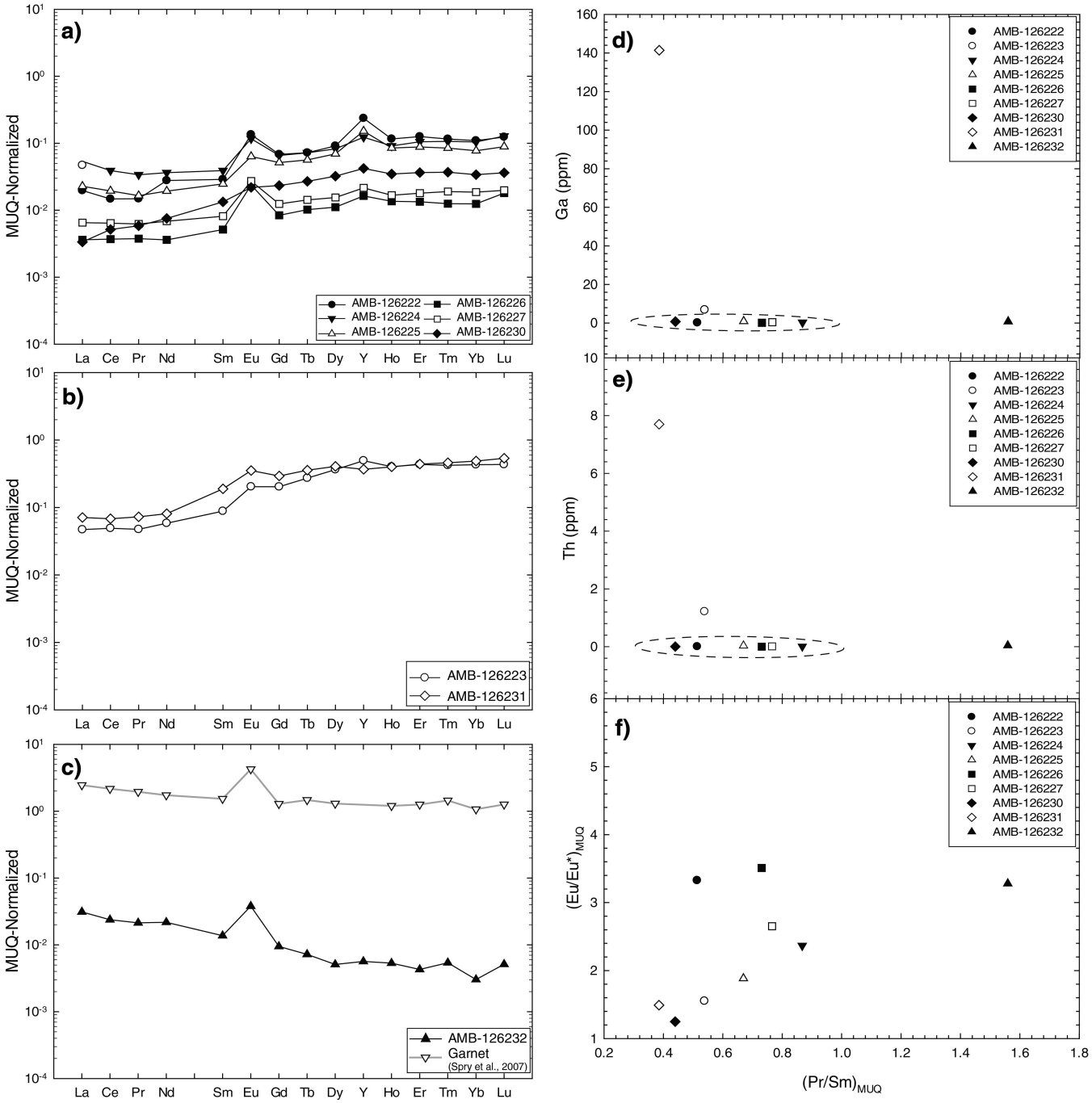

Figure 7. MUQ-normalized REE patterns for the Central BIF partition showing **a)** ambient seawater and hydrothermal input, **b)** atypical REE+Y showing contamination, and **c)** Atypical REE+Y showing artifact effect of garnet; **d)** Ga vs. Pr/Sm_{MUQ}; **e)** Th vs. Pr/Sm_{MUQ}; **f)** Eu/Eu*MUQ vs. Pr/Sm_{MUQ}

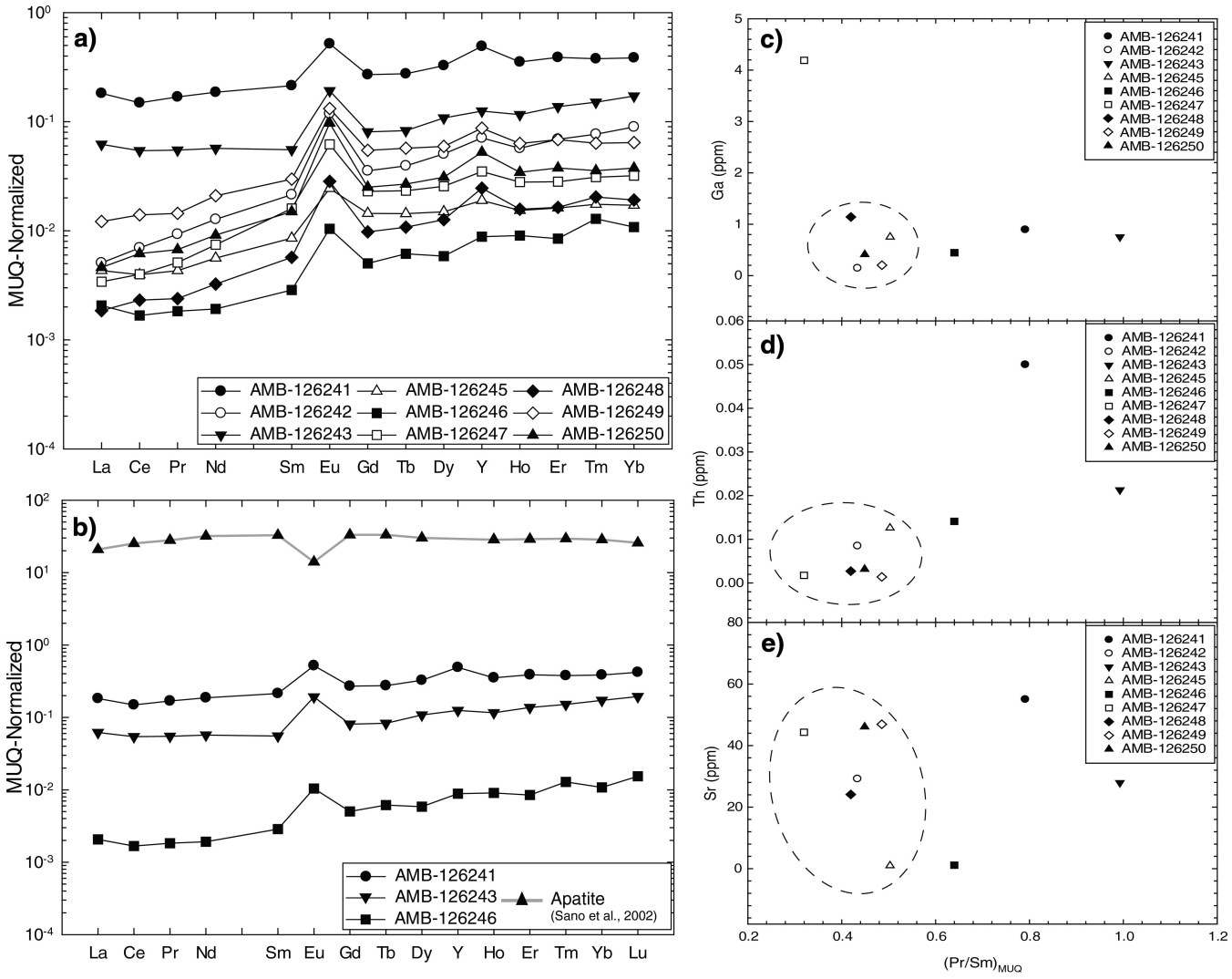

Figure 8. MUQ-normalized REE patterns for the East IF partition showing **a)** ambient seawater and hydrothermal input, **b)** atypical REE+Y showing contamination; **c)** Ga vs. Pr/Sm_{MUQ}, **d)** Th vs. $Pr/Sm_{MUQ,}$ and **e)** Sr vs. Pr/Sm_{MUQ}

Based on only two samples, the Grizzly data show a very consistent pattern with a strong enrichment in HREEs relative to MREEs and LREEs (Nd/Yb_{MUQ} = 0.07–0.1), positive Gd, La, Y, and Eu anomalies (Gd/Gd^*_{MUQ} = 1–1.1, La/La^*_{MUQ} = 1.6, Y/Y^*_{MUQ} = 1.1–1.3 and Eu/Eu^*_{MUQ} = 2.3–3.5) (Fig. 5e). Moreover, the Grizzly area is noted to be surrounded by a batholith dated at ca. 2.612 ± 4 Ma which could have affected the older BIF (interpreted as coeval with bimodal volcanism) due to later hydrothermal alteration.

Summary and Discussion

The Meadowbank gold deposit consists of several Algoma-type BIFs which differ in their petrography and geochemistry. Preliminary trace-element geochemical data for the BIFs at Meadowbank is used to constrain the origin of these units as well as assess the effect of such geochemical characteristics on the formation of BIF-hosted gold deposits.

The Far West BIF is not mineralized with the exception of a 2.8 g/t Au over 3.6 m interval in a very restricted area (Agnico-Eagle Mines Ltd, 2012). Most of the samples from this BIF were not discussed here as the very low levels of REEs produced very erratic REE_{MUQ} normalized patterns. However, this characteristic may be due to reworking after deposition.

The West BIF is barren except for a few weakly anomalous gold values (Agnico-Eagle Mines Ltd, 2012). The geochemical data show very consistent REE patterns which reflect the influence of ambient seawater with some hydrothermal input. Some chert bands are affected by crustal contamination, as represented by the levels of Ga (i.e. a proxy for aluminum), Th, and Sr (i.e. a proxy for phosphates).

The Central BIF is the more mineralized BIF in the Meadowbank area and contains 24.5 Mt proven/probable ore reserves grading to 2.8 g/t (2011 data) (Agnico-Eagle pers. comm., 2012). The geochemistry for this BIF shows

the influence of ambient seawater and hydrothermal input, but some chert bands reflect crustal contamination, again characterized by elevated Ga (i.e. proxy of aluminum) and Th.

The East BIF, considered mostly barren except for an isolated intersection at 3.23 g/t Au over 2.7 m (Agnico-Eagle Mines Ltd, 2012), is located to the east of the Central BIF. It shows very similar REE patterns to the West IF with ambient seawater and hydrothermal input, as well as crustal contamination showing approximately the same pattern as the Central and West IF with a low content of Ga (i.e. proxy of aluminum), Th and Sr (i.e. proxy for phosphates).

Located at the extreme east of the property, the Grizzly BIF shows homogeneous very weak gold mineralization (one intersection averaging of 0.20 g/t over 49 m) with some richer intersections (0.96 g/t over 24 m including 7.44 g/t over 2.6 m) (Agnico-Eagle pers. comm. 2012). This BIF shows very distinctive REE patterns with very significant enrichment in HREEs relative to LREEs and a strong positive Eu anomaly. This pattern suggests, therefore, an ambient seawater signature associated with or overprinted by a strong hydrothermal input. The nature of the pronounced hydrothermal signal in the BIF at Grizzly is perhaps of a secondary nature as 1) the sampled area is located near a much younger massive granite, 2) it contains significant gold, and 3) it is associated with a particular alteration (i.e.,) that is uncommon in the region. Thus, for these aforementioned reasons it is suggested that the history of this BIF is different from that of the other gold-bearing and barren BIFs in the region and that it might have been influenced by the nearby intrusions.

Consequently, the BIFs show different geochemical signatures based on ICP-MS ablation analyses and suggest ambient seawater and hydrothermal input associated with some crustal contamination. We use three measures of the prominence of oceanic processes Nd/Yb, La/La* and Y/Ho to gauge the degree of control of REE+Y geochemistry of the BIF at Meadowbank by oceanic processes. The Nd/Yb values for the West BIF (0.042–2.170) are greater than those for the East BIF (0.142–0.484) and the Central BIF (0.135–0.484). Thus the West BIF was likely deposited in deeper water than either the Central or the East BIF. La/La*, Gd/Gd*, and Y/Ho are broadly positive indicating a hydrogenous sedimentary signature. Most samples in this study also show weakly positive values for Eu/Eu* (1.24–5.12) indicating a hydrothermal overprint on the hydrogenous signature. It should be noted that the hydrothermal overprint (Eu/Eu*) for the Meadowbank BIFs is not as high as that recorded for the BIFs above the Deloro assemblage (e.g. 30+) in the Abitibi greenstone belt (Thurston et al., 2012). West BIF and East BIF show similar REE patterns and could be folded equivalents of the same unit with the western unit perhaps representing deeper water based on Nd/Yb values listed above using the criteria of Kamber (2010).

Thus in terms of REE+Y geochemistry, there are no major differences between mineralized and unmineralized BIFs at Meadowbank. However our study has not yet examined indicators of any organic influence on BIF development, the effects of early vs. late sulphides and the overall oxidation state of the BIF on the mineralizing processes.

Based on this new geochemical data, the next step in this project will be to examine stratigraphic trends from this deposit, to compare samples from the Musselwhite, Meliadine, and MacLeod-Cockshutt deposits and also to analyze samples using the ICP-MS solution method for comparison with recent studies (e.g. Baldwin, 2009) and permitting improvement of detection limits.

ACKNOWLEDGMENTS

The authors gratefully acknowledge the staff of Agnico Eagle Mines Ltd. and more particularly the Meadowbank regional exploration crew supervised by Olivier Côté-Mantha for the help and logistics provided for the project. The authors also thank Dr. Sally Pehrsson of the Geological Survey of Canada for discussions regarding the regional geological setting of the study area, and Mr. Vivien Janvier of the INRS-ETE for discussions on the geological setting of the Meadowbank deposit.

REFERENCES

Agnico-Eagle Mines Ltd, 2008. Technical Report on the mineral resources and mineral reserves, Meadowbank gold project, Nunavut, Canada; report prepared by L. Connell, D. Doucet, A. Fortin, J. Hettinger, E. Lamontagne, and B. Perron, 169 p.

Agnico-Eagle Mines Ltd, 2012. Technical report on the mineral resources and mineral reserves, Meadowbank gold project, Nunavut, Canada; report prepared for Agnico Eagle Mines Ltd. By Ruel, M., Proulx, A., Muteb, P.N., and Connell, L., 190 p.

Alexander, B.W., Bau, M., Andersson, P., and Dulski, P., 2008. Continentally-derived solutes in shallow Archean sea water; rare earth element and Nd isotope evidence in iron formation from the 2.9 Ga Pongola Supergroup, South Africa; Geochimica et Cosmochimica Acta, v. 72, p. 378–394. doi:10.1016/j.gca.2007.10.028

Allwood, A.C., Kamber, B.S., Walter, M.R., Burch, I.W., and Kanik, I., 2010. Trace element record depositional history of an Early Archean stromatolitic carbonate platform; Chemical Geology, v. 270, p. 148–163. doi:10.1016/j.chemgeo.2009.11.013

Annesley, I.R., 1989. Petrochemistry of the Woodburn Lake group komatiite suite, Amer Lake, N.W.T., Canada; Ph.D. thesis, University of Ottawa, Ottawa, Ontario, 406 p.

Armitage, A.E., James, R.S., and Goff, S.P., 1996. Gold mineralization in Archean banded iron formation, Third Portage Lake area, Northwest Territories, Canada; Exploration and Mining Geology, v. 5, no. 1, p. 1–15.

Ashton, K.E., 1985. Archean orthoquartzites from the Churchill Structural Province near Baker Lake, N.W.T.; Geological Association of Canada, Mineralogical Association of Canada; Program with Abstracts (Geological Association of Canada), v. 10, p. A2.

Aspler, L.B. and Chiarenzelli, J.R., 1996. Stratigraphy, sedimentology and physical volcanology of the Henik Group, central Ennadai-Rankin greenstone belt, Northwest Territories, Canada: Late Archean paleogeography of the Hearne Province and tectonic implications; Precambrian Research, v. 77, p. 59–89. doi:10.1016/0301-9268(95)00045-3

Baldwin, G.J., 2009. The sedimentology and geochemistry of banded iron formations of the Deloro Assemblage, Bartlett Dome area, Abitibi greenstone belt, Ontario, Canada: Implications for BIF deposition and greenstone belt formation, Earth Sciences; MSc thesis, Laurentian University, Sudbury, Ontario, 116 p.

Bau, M. and Alexander, B.W., 2009. Distribution of high field strength elements (Y, Zr, REE, Hf, Ta, Th, U) in adjacent magnetite and chert bands and in reference standards FeR-3 and FeR-4 from the Temagami iron-formation, Canada, and the redox level of the Neoarchean ocean; Precambrian Research, v. 174, p. 337–346.

Bau, M. and Dulski, P., 1996. Distribution of Y and rare-earth elements in the Penge and Kuruman Iron Formations, Transvaal Supergroup, South Africa; Precambrian Research, v. 79, p. 37–55. doi:10.1016/0301-9268(95)00087-9

Biczok, J., Hollings, P., Klipfel, P., Heaman, L., Maas, R., Hamilton, M., Kamo, S., and Friedman, R., 2012. Geochronology of the North Caribou greenstone belt, Superior Province Canada: Implications for tectonic history and gold mineralization at the Musselwhite mine; Precambrian Research, v. 192-195, p. 209–230.

Bolhar, R., Van Kranendonk, M.J., and Kamber, B.S., 2005. A trace element study of siderite-jasper banded iron formation in the 3.45 Ga Warrawoona Group, Pilbara craton-Formation from hydrothermal fluids and shallow seawater; Precambrian Research, v. 137, p. 93–114. doi:10.1016/j.precamres.2005.02.001

Carpenter, R.L., Duke, N.A., Sandeman, H.A., and Stern, R., 2005. Relative and absolute timing of gold mineralization along the Meliadine Trend, Nunavut, Canada; evidence for Paleoproterozoic gold hosted in an Archean greenstone belt; Economic Geology and the Bulletin of the Society of Economic Geologists, v. 100, p. 567–576.

Castonguay, S., Janvier, V., Mercier-Langevin, P., Dubé, B., McNicoll, V., Malo, M., Pehrsson, S., and Bécu, V., 2012, Recognizing optimum banded-iron formation-hosted gold environments in ancient, deformed and metamorphosed terranes: Preliminary results from the Meadowbank deposit, Nunavut: 40th Annual Yellowknife Geoscience Forum, Yellowknife, NWT, November 15–17.

Clout, J.M.F. and Simonson, B.M., 2005. Precambrian Iron Formations and Iron Formation-Hosted Iron Ore Deposits; *in* Economic Geology One Hundredth Anniversary Volume, (ed.) J.W. Hedenquist, J.F.H. Thompson, R.J. Goldfarb, and J.P. Richards; Society of Economic Geologists, Littleton, CO, p. 643–680.

Danielson, A., Moeller, P., and Dulski, P., 1992. The europium anomalies in banded iron formations and the thermal history of the oceanic crust; Chemical Geology, v. 97, p. 89–100. doi:10.1016/0009-2541(92)90137-T

Davis, W.J. and Zaleski, E., 1998. Geochronological investigations of the Woodburn Lake group, western Churchill province, Northwest Territories: Preliminary results; Radiogenic Age and Isotopic Studies: Report 11; *in* Current Research 1998-F, Geological Survey of Canada, p. 89–97.

Dubé, B. and Gosselin, P., 2007. Greenstone-hosted quartz-carbonate vein deposits; *in* Mineral Deposits of Canada: a synthesis of major deposit types, district metallogeny, the evolution of geological provinces, and exploration methods, (ed.) W.D. Goodfellow; Geological Association of Canada, Mineral Deposits Division, Special Publication 5, p. 49–73.

Eriksson, P.G., Martins-Neto, M.A., Nelson, D.R., Aspler, L.B., Chiarenzelli, J.R., Catuneanu, O., Sarkar, S., Altermann, W., De, W., and Rautenbach, J.C., 2001. An introduction to Precambrian basins: their characteristics and genesis; Sedimentary Geology, v. 141–142, p. 1–35. doi:10.1016/S0037-0738(01)00066-5

Fralick, P. and Pufahl, P.K., 2006. Iron formation in Neoarchean deltaic successions and the microbially mediated deposition of transgressive systems tracts; Journal of Sedimentary Research, v. 76, p. 1057–1066. doi:10.2110/jsr.2006.095

Frei, R., Dahl, P.S., Duke, E.F., Hansen, T.R., Frandsson, M.M., and Jensen, L.A., 2008. Trace element and isotopic characterization of Neoarchean and Paleoproterozoic iron formations in the Black Hills (South Dakota USA): assessment of chemical change during 2.9-1.9 Ga deposition bracketing the 2.4-2.2 Ga first rise of atmospheric oxygen; Precambrian Geology, v. 162, p. 441–474.

Goldfarb, R.J., Groves, D.I., and Gardoll, S., 2001. Orogenic gold and geologic time: A global synthesis; Ore Geology Reviews, v. 18, p. 1–75. doi:10.1016/S0169-1368(01)00016-6

Gross, G.A., 1965. Geology of iron deposits in Canada; general geology and evaluation of iron deposits; Geological Survey of Canada, Economic Geology Report 22, 181 p.

Hall, R.S. and Rigg, D.M., 1986. Geology of the West Anticline Zone, Musselwhite Prospect, Opapimiskan Lake, Ontario, Canada; *in* Gold '86; an international symposium on the geology of gold deposits; proceedings volume; GOLD '86, (ed.) A.J. Macdonald Toronto, ON, Canada, p. 124–136.

Hanor, J.S. and Duchac, K.C., 1990. Isovolumetric silicification of early Archean komatiites; geochemical mass balances and constraints on origin; The Journal of Geology, v. 98, p. 863–877. doi:10.1086/629458

Henderson, J.R. and Henderson, M.N., 1994. Geology of the Whitehills-Tehek Lakes area, District of Keewatin, Northwest Territories (parts of 56D, 56E, 66A and 66H); Geological Survey of Canada, Open File 2923, scale 1:100 000.

Henderson, J.R., Henderson, M.N., Pryer, L.L., and Cresswell, R.G., 1991. Geology of the Whitehills-Tehek area, District of Keewatin: An Archean supracrustal belt with iron-formation hosted gold mineralization in the central Churchill province; *in* Current Research Part C, Geological Survey of Canada, Paper 91-1C, p. 149–156.

Hoffman, P.F., 1989. Precambrian geology and tectonic history of North America; *in* The Geology of North America–An overview, (ed.) A.W. Bally and A.R. Palmer; Geological Society of America, The Geology of North America, Part A, p. 447–512.

Hrabi, R.B., Barclay, W.A., Fleming, D., and Alexander, R.B., 2003. Structural evolution of the Woodburn Lake group in the area of the Meadowbank gold deposit, Nunavut; Current Research 2003-C27; Geological Survey of Canada; 10 p. doi:10.4095/214396

Janvier, V., Castonguay, S., Mercier-Langevin, P., Dubé, B., McNicoll, V., Malo, M., Pehrsson, S., and Bécu, V., 2013, Recognizing optimum banded-iron formation hosted gold environments in ancient, deformed and metamorphosed terranes: Preliminary results from the Meadowbank deposit, Nunavut; Geological Survey of Canada, Open File 7407, poster. doi:10.4095/292589

Kamber, B.S., 2010. Archean mafic-ultramafic volcanic landmasses and their effect on ocean-atmosphere chemistry; Chemical Geology, v. 274, p. 19–28. doi:10.1016/j.chemgeo.2010.03.009

Kamber, B.S. and Webb, G.E., 2007. Transition metal abundances in microbial carbonate: a pilot study based on in situ LA-ICP-MS analysis; Geobiology, v. 5, p. 375–389. doi:10.1111/j.1472-4669.2007.00129.x

Kamber, B.S., Bolhar, R., and Webb, G.E., 2004. Geochemistry of late Archaean stromatolites from Zimbabwe: evidence for microbial life in restricted epicontinental seas; Precambrian Research, v. 132, p. 379–399. doi:10.1016/j.precamres.2004.03.006

Kerswill, J.A., 1993. Models for iron-formation-hosted gold deposits; *in* Mineral Deposit Modeling, (ed.)R.V. Kirkham, W.D. Sinclair, R.I. Thorpe, and J.M. Duke; Geological Association of Canada, Special Paper 40, p. 171–199.

Kerswill, J.A., 2000. Iron-formation-hosted gold deposits: a view from Nunavut with emphasis on "Lupin-like" deposits; *in* Abstract Volume, Short Course on Geology and Mineral Deposits of Nunavut Territory; Society of Economic Geologists, London Student Chapter, March 3, 2000, 10 p.

Kerswill, J.A., Goff, S.P., Wilkinson, L., Jenner, G.A., Kjarsgaard, B.A., Bretzlaff, R., and Samaras, C., 1998. An update on the metallogeny of the Woodburn Lake group, western Churchill province, Northwest Territories; *in* Current Research 1998-C; Geological Survey of Canada; p. 29–41. doi:10.4095/209511

Kerswill, J.A., Goff, S.P., Kjarsgaard, B.A., Jenner, G.A. and Wilkinson, L. 2000. Highlights of recent metallogenic investigations in western Churchill province, Nunavut, Canada: Implications for mineral exploration in Archean greenstone belts; in GeoCanada 2000 — The Millennium Geoscience Summit CD-ROM, Calgary, Abstract 736.

Kuehn, S., 1990. The Geita gold mine, Tanzania, and its metallogenetic position; Proceedings of the Quadrennial IAGOD Symposium 8, A272-A273.

Ladeira, E.A., 1991. Genesis of Gold in the quadrilatero Ferrifero -A remarkable case of permanency, recycling and inheritance - a tribute to Djalma Guimaraes, Pierre Routhier, and Hans Ramberg; *in* Brazil Gold '91 - the geology, geochemistry and genesis of gold deposits, (ed.) E.A. Ladeira; Balkema, Rotterdam, p. 11–30.

Lafrance, B., DeWolfe, J.C., Stott, G.M., 2004. A structural reappraisal of the Beardmore-Geraldton Belt at the southern boundary of the Wabigoon Subprovince, Ontario, and implications for gold mineralization; Canadian Journal of Earth Sciences = Revue Canadienne des Sciences de la Terre 41, p. 217–235.

Lascelles, D.F., 2007. Black smokers and density currents; an uniformitarian model for the genesis of banded iron formations; Ore Geology Reviews, v. 32, p. 381–411. doi:10.1016/j.oregeorev.2006.11.005

Lawrence, M.G. and Kamber, B.S., 2005. The behavior of the rare earth elements during estuarine mixing- revisited; Marine Chemistry, v. 100, p. 147–161.

Macdonald, A.J., 1988. The Geraldton Gold Camp: the Role of Banded Iron Formation; Ontario Geological Survey, Open File 5694, 173 p.

Miller, A.R. and Tella, S., 1995. Stratigraphic settings of semiconformable alteration in the Spi Lake area, Kaminak greenstone belt, Churchill province, Northwest Territories; *in* Current Research 1995-C; Geological Survey of Canada; p. 175–186.

Pehrsson, S., Wilkinson, L., Zaleski, E., Kerswill, J., and Alexander, R.B., 2000. Structural geometry of the Meadowbank deposit area, Woodburn Lake group—implications for a major gold deposit in the western Churchill province; *in* GeoCanada 2000—The Millennium Geoscience Summit CD-ROM, (abstract).

Pehrsson, S.J., Wilkinson, L., and Zaleski, E., 2004. Geology of the Meadowbank gold deposit area, Nunavut; Geological Survey of Canada, Open File 4269, scale 1:20 000.

Planavsky, N., Bekker, A., Rouxel, O.J., Kamber, B.S., Hofmann, A.W., Knudsen, A., and Lyons, T.W., 2010. Rare Earth Element and yttrium compositions of Archean and paleoproterozoic Fe formations revisited: New perspectives on the significance and mechanisms of deposition; Geochimica et Cosmochimica Acta, v. 74, p. 6387–6405.

Roddick, J.C., Henderson, J.R., and Chapman, H.J., 1992. U-Pb ages from the Archean Whitehills-Tehek Lakes Supracrustal Bell, Churchill Province, District of Keewatin, Northwest Territories; *in* Radiogenic Age and Isotopic Studies: Report 6, Geological Survey of Canada, Paper 1992–2, p. 31–40.

Sano, Y., Terada, K., and Fukuoka, T., 2002. High mass resolution ion microprobe analysis of rare earth element in silicate glass, apatite and zircon: lack of matrix dependency; Chemical Geology, v. 184, p. 217–230. doi:10.1016/S0009-2541(01)00366-7

Schau, M., 1982. Geology of the Prince Albert Group in parts of Walker Lake and Laughland Lake map areas, District of Keewatin; Geological Survey of Canada, Bulletin 337, 62 p.

Schau, M. and Ashton, K.E., 1988. The Archean Prince Albert Group, Northeastern Canada: Evidence for crustal extension within >2.9 Ga continent; Geological Society of America; Program with Abstracts (Geological Association of Canada), v. 20, p. A50.

Sherlock, R.L., Alexander, R.B., March, R., and Barclay, W.A., 2001a. Geologic setting of the Meadowbank iron formation-hosted gold deposits; Current Research 2001-C11; Geological Survey of Canada; 23 p. doi:10.4095/212081

Sherlock, R.L., Alexander, R.B., March, R., and Barclay, W.A., 2001b. Geologic setting of the Meadowbank iron formation-hosted gold deposits; Geological Survey of Canada, Open File 3149, scale 1:10 000.

Sherlock, R.L., Pehrsson, M.S., Logan, A.V., Hrabi, R.B., and Davis, W.J., 2004. Geological Setting of the Meadowbank Gold Deposits, Woodburn Lake Group, Nunavut; Exploration and Mining Geology, v. 13, no. 1–4, p. 67–107. doi:10.2113/gsemg.13.1-4.67

Spry, P.G., Messerly, J.D., and Houk, R.S., 2007. Discrimination of metamorphic and metasomatic processes at the Broken Hill Pb-Zn-Ag deposit, Australia: rare earth element signature of garnet-rich rocks; Economic Geology and the Bulletin of the Society of Economic Geologists, v. 102, p. 471–494. doi:10.2113/gsecongeo.102.3.471

Tella, S., Hanmer, S., Sandeman, H.A., Ryan, J.J., Mills, A., Davis, W.J., Berman, R.G., Wilkinson, L., and Kerswill, J.A., 2001. Geology, MacQuoid Lake-Gibson Lake-Akunak Bay area, Nunavut; Geological Survey of Canada, Map 2008A, scale 1:100 000. doi:10.4095/212827

Thurston, P.C., Kamber, B.S., and Whitehouse, M., 2012. Archean cherts in banded iron formation: insight into Neoarchean ocean chemistry and depositional processes; Precambrian Research, v. 214–215, p. 227–257. doi:10.1016/j.precamres.2012.04.004

Wilkinson, L., Pehrsson, S., Zaleski, E., Kerswill, J., and Alexander, R.B., 2000. Woodburn Lake Group: Structural Geometry of the Meadowbank Deposit Area – Implications for Genesis of a Major Gold Deposit in the Western Churchill Province; 28th Yellowknife Geoscience Forum, November 2000, Program (abstracts).

Zaleski, E., Corrigan, D., Kjarsgaard, B.A., Kerswill, J.A., Jenner, G.A., and Henderson, J.R., 1997a. Geology, Woodburn Lake group, Meadowbank River to Tehek Lake (66 H/1, 56 E/4), District of Keewatin (Nunavut), Northwest Territories; Geological Survey of Canada, Open File 3461, scale 1:50 000. doi:10.4095/208990

Zaleski, E., Corrigan, D., Kjarsgaard, B.A., Kerswill, J.A., Jenner, G.A., and Henderson, J.R., 1997b. Preliminary results of mapping and structural interpretation from the Woodburn project, western Churchill province, Northwest Territories; *in* Current Research 1997-C; Geological Survey of Canada; p. 91–100.

Zaleski, E., Duke, N.L., L'Heureux, R., and Wilkinson, L., 1999a. Geology, Woodburn Lake group, Amarulik Lake to Tehek Lake, Kivalliq Region, Nunavut; Geological Survey of Canada, Open File 3743, scale 1:50 000. doi:10.4095/210634

Zaleski, E., L'Heureux, R., Duke, N., Wilkinson, L., and Davis, W.J., 1999b. Komatiitic and felsic volcanic rocks overlain by quartzite, Woodburn Lake group, Meadowbank River Area, western Churchill province, Northwest Territories (Nunavut); *in* Current Research 1999-C, Geological Survey of Canada, p. 9–18.

Zaleski, E., Davis, W.J., and Wilkinson, L., 2000. Basement / cover relationships, unconformities and depositional cycles of the Woodburn Lake group, western Churchill province Nunavut; 28th Yellowknife Geoscience Forum, November 2000, Program (abstracts).

Zaleski, E., Davis, W.J., and Sandeman, H.A., 2001. Continental extension, mantle magmas basement/cover relationships; Record - Australian Geological Survey Organisation, p. 374–376.

Geological Survey of Canada Project 340331NU61